

Possible Existence of Extremely Neutron-Rich Superheavy Nuclei in Neutron Star Crusts Under a Superstrong Magnetic Field

Kazuyuki Sekizawa^{1,2,3,*} and Kentaro Kaba¹

¹*Department of Physics, School of Science, Tokyo Institute of Technology, Tokyo 152-8551, Japan*

²*Nuclear Physics Division, Center for Computational Sciences, University of Tsukuba, Ibaraki 305-8577, Japan*

³*RIKEN Nishina Center, Saitama 351-0198, Japan*

(Dated: February 16, 2023)

We investigate outer crust compositions for a wide range of magnetic field strengths, up to $B \simeq 4 \times 10^{18}$ G, employing the latest experimental nuclear masses supplemented with various mass models. The essential effects of the magnetic field are twofolds: 1) Enhancement of electron fraction, which is connected to that of protons via the charge neutrality condition, due to the Landau-Rabi quantization of electron motion perpendicular to the field, namely, neutron-richness is suppressed for a given pressure. As a result, 2) nuclei can exist at higher pressures without dripping out neutrons. By exploring optimal outer-crust compositions from all possible nuclei predicted by theoretical models, we find that neutron-rich heavy nuclei with neutron magic numbers 50, 82, 126, as well as 184, with various proton numbers emerge for $B \gtrsim 10^{17}$ G. Moreover, we show that superheavy nuclei with proton numbers $Z \geq 104$, including unknown elements such as $Z = 119, 120, 122$, and/or 124 , depending on mass models, may emerge as an equilibrium composition at bottom layers of the outer crust for $B \gtrsim 10^{18}$ G, which are extremely neutron-rich ($N \approx 260\text{--}287$, *i.e.*, $N/Z \approx 2.2\text{--}2.4$). We point out that those extremely neutron-rich superheavy nuclei locate around the next neutron magic number $N = 258$ after $N = 184$, underlining importance of nuclear structure calculations under such really exotic, extreme conditions. We demonstrate how the superstrong magnetic field substantially alters crustal properties of neutron stars, which may have detectable consequences.

Introduction.—What is the heaviest element that can, if it is very short lived, exist in nature? This simple, yet profound question has urged us to synthesize unknown superheavy nuclei (SHN) at terrestrial accelerator facilities all over the world [1–5]. The synthesis of SHN is notoriously difficult due to its really tiny cross sections on the order of picobarn to femtobarn. Nevertheless, owing to the continuous endeavor for synthesizing SHN, the elements up to the atomic number $Z = 113$, nihonium, and $Z = 118$, oganesson, have been synthesized so far via the so-called cold and hot fusion reactions, respectively. Although the artificially synthesized SHN are short-lived, their chemical as well as nuclear properties are of great interests, offering a unique opportunity to challenge our theoretical understanding. The ever-ending quest for the next unknown elements 119, 120, and beyond, is the most challenging subject in nuclear physics today. In this Letter we show that extremely neutron-rich (N -rich) SHN, including the yet unknown elements, may naturally exist as an equilibrium composition of solid crusts of strongly-magnetized neutron stars; see Fig. 1.

Neutron stars are known to sustain a very strong magnetic field. The surface magnetic field in the majority of pulsars is about $B \approx 10^{11}\text{--}10^{13}$ G, but some radio pulsars exhibit larger magnetic fields on the order of $10^{13}\text{--}10^{14}$ G [9]. Further, from observations of soft γ -ray repeaters (SGRs) and anomalous x-ray pulsars (AXPs), stronger surface magnetic fields up to 2.4×10^{15} G have been inferred [10–14]. According to the virial theorem and magnetohydrodynamics simulations, the upper limit on the neutron-star magnetic fields could be on the order of $B \approx 10^{18}$ G [15–18]. Although it would be a rare situation, it is worth exploring neutron star properties under such an extreme condition, prior to possible observational finding. In this work, we thus focus on effects of a magnetic

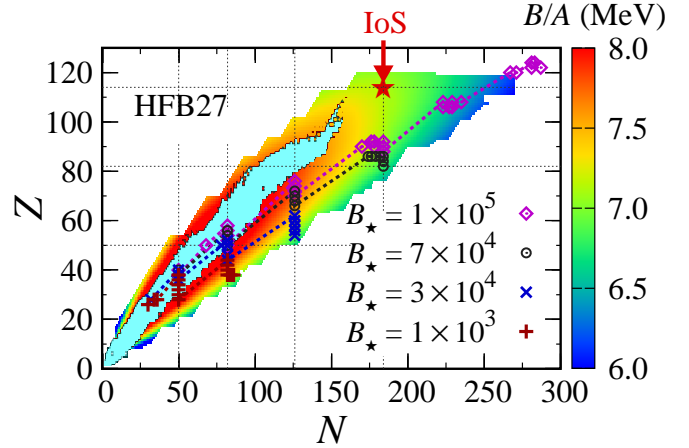


FIG. 1. The main finding of this Letter. Colored area shows binding energy per nucleon (B/A in MeV) predicted by the microscopic HFB-27 mass model [6]. Shaded area indicates the region where experimental masses are available in AME2020 [7, 8]. On top of that, calculated equilibrium compositions of the outer crust in strongly-magnetized neutron stars are plotted for $B_* = 10^5$ (diamonds), 7×10^4 (circles), 3×10^4 (crosses), and 10^3 (plus symbols), where $B_* = B/B_c$ with $B_c \simeq 4.4 \times 10^{13}$ G. Dotted lines connect those symbols to guide the eye. Vertical (horizontal) dotted lines indicate neutron (proton) spherical magic numbers, $N = 50, 82, 126$, and 184 ($Z = 50, 82$, and 114). The *island of stability* (IoS) located around $Z = 114$ and $N = 184$ is indicated by a star. Emergence of extremely N -rich nuclei is clearly exhibited (see texts for details).

field on the outer crust compositions up to the extreme condition, $B \gtrsim 10^{18}$ G, instead of higher density regions where filling of higher Landau levels weakens the effects.

Effects of a magnetic field on outer crust compositions have been studied with various models, such as Thomas-Fermi model [19], liquid drop model [20], Nilsson model [21, 22],

covariant (relativistic) density functional theory (CDFT) [23, 24], Skyrme (non-relativistic) DFT [25, 26], effective relativistic mean-field model [27]. The common understanding is that the most significant effect of a magnetic field originates from the Landau-Rabi quantization of electron motion perpendicular to the field [28, 29]. In addition, nuclear structure could be affected for $B \gtrsim 10^{17}$ G, where spin-dependent shifts of single-particle energies become on the order of MeV [23, 24, 30, 31]. In such a case, the size of shell gaps and even the ordering of energy levels may be altered and, as a result, structural properties, such as deformation, radius, mass, could be affected. However, the studies carried out so far are limited to a relatively light mass region, below or around Fe up to around Xe [27] or so, probably because nuclides treated as candidates of an equilibrium composition were somehow restricted.

In this Letter, we shall extend the investigation along the line with Ref. [25], adopting the latest experimental masses, AME2020 [7, 8], supplemented with various mass models (HFB-27 [6], HFB-32 [32], BML [33], and KTUY [34]). We carry out a comprehensive search for the equilibrium compositions from all nuclei in the entire nuclear chart, *i.e.* until the drip lines including SHN, for a wide range of magnetic field strengths. We show that extremely N -rich SHN are allowed to exist as an equilibrium composition of bottom layers of the outer crust of strongly-magnetized neutron stars. We mention here that similar possibilities of emergence of SHN have been discussed in the context of supernova explosions, where large electron fractions could be realized in an explosive situation (see, *e.g.*, Ref. [35]). We discuss significant changes of crustal properties caused by the superstrong magnetic field, which may have detectable consequences.

Method.— The most significant effect of the magnetic field is caused by the Landau-Rabi quantization of electron motion perpendicular to the field [28, 29]. The Landau energy level of relativistic electrons is given by $E_\nu(p_z, B_\star) = \sqrt{p_z^2 c^2 + m_e^2 c^4 (1 + 2\nu B_\star)}$ with $\nu = n_L + \frac{1}{2} + \sigma$, where ν is the quantum number of the Landau levels, n_L is a non-negative integer number, $p_z = \hbar k_z$ is electron momentum along the magnetic field, $\sigma = \pm 1/2$ represents the spin degrees of freedom, m_e is the electron mass, c is the speed of light, and $B_\star \equiv B/B_c$ (see, *e.g.*, Ref. [36]). It is customary to quantify the magnetic field strength relative to the critical value, $B_c = m_e^2 c^3 / e \hbar \simeq 4.41 \times 10^{13}$ G, at which the cyclotron energy of electrons reaches its rest mass energy. The electron number density, n_e , energy density, \mathcal{E}_e , and pressure, P_e , are given by

$$n_e = \frac{2B_\star}{(2\pi)^2 \lambda_e^3} \sum_{\nu=0}^{\nu_{\max}} g_\nu x_e(\nu, B_\star), \quad (1)$$

$$\mathcal{E}_e = \frac{B_\star m_e c^2}{(2\pi)^2 \lambda_e^3} \sum_{\nu=0}^{\nu_{\max}} g_\nu (1 + 2\nu B_\star) \psi_+ \left[\frac{x_e(\nu, B_\star)}{\sqrt{1 + 2\nu B_\star}} \right], \quad (2)$$

$$P_e = \frac{B_\star m_e c^2}{(2\pi)^2 \lambda_e^3} \sum_{\nu=0}^{\nu_{\max}} g_\nu (1 + 2\nu B_\star) \psi_- \left[\frac{x_e(\nu, B_\star)}{\sqrt{1 + 2\nu B_\star}} \right], \quad (3)$$

where $\lambda_e = \hbar / m_e c$ is the electron Compton wavelength, g_ν

represents the degeneracy ($g_\nu = 1$ for $\nu = 0$ and 2 for $\nu \geq 1$), $x_e(\nu, B_\star) = \sqrt{\gamma_e^2 - (1 + 2\nu B_\star)}$ with $\gamma_e = \mu_e / m_e c^2$, the electron chemical potential relative to the electron rest mass energy, $\psi_\pm[x] = x\sqrt{1+x^2} \pm \ln(x + \sqrt{1+x^2})$, and ν_{\max} denotes the highest occupied Landau level that satisfies $E_{\nu_{\max}}(p_z=0, B_\star) \leq \mu_e$.

To determine the outer crust composition under a magnetic field, we employ the method of Baym, Pethick, and Sutherland [37] (which we call the BPS method below). In the BPS method, the Gibbs energy per nucleon, $g = (\mathcal{E}_{\text{WS}} + P)/n$, is minimized for a given pressure P and a magnetic field strength B , where \mathcal{E}_{WS} is the energy density of the Wigner-Seitz cell and n is the average baryon (nucleon) number density. The Gibbs energy per nucleon reads¹

$$g(A, Z; P, B) = \frac{M'(A, Z)c^2}{A} + \frac{Z}{A} \left(\frac{4\mathcal{E}_L}{3m_e} + \mu_e \right), \quad (4)$$

where $M'(A, Z)$ is the mass of an atomic nucleus with a mass number A and a proton number Z . We adopt the latest experimental data, AME2020 [7, 8], whenever available. Note that in an ordinary outer crust all nuclei are pressure ionized and the nuclear masses (not the atomic ones) should be used, correcting the tabulated experimental atomic masses, $M(A, Z)$, as $M'(A, Z)c^2 = M(A, Z)c^2 - Zm_e c^2 + B_e(Z)$, where $B_e(Z)$ denotes the binding energy of electrons². When experimental masses are not available, we adopt those predicted by a theoretical mass model. We employ two variants of a microscopic mass model based on the Hartree-Fock-Bogoliubov (HFB) theory (HFB-27 [6] and HFB-32 [32]), the most accurate mass model to date which employs the Bayesian Machine Learning (BML) [33], and a phenomenological mass model (KTUY [34]). We note that the pressure ionization may be hindered in the presence of a strong magnetic field, which may introduce certain corrections to the atomic masses. In this work we disregard the effects of a magnetic field on nuclear masses, as in Ref. [25]. As will be discussed below, inclusion of the latter effects on nuclear masses will strengthen our finding. \mathcal{E}_L is the lattice part of energy density, $\mathcal{E}_L = -C_M (4\pi/3)^{1/3} Z^2 e^2 n_{\text{nuc}}^{4/3}$, where C_M is the so-called Madelung constant specific to the lattice. According to the values of C_M [40]³, a BCC lattice is favored. n_{nuc} is the number density of nuclei, which is given by $n_{\text{nuc}} = n/A = n_p/Z = 1/V_{\text{WS}}$, where n_p is the proton number density and V_{WS} denotes the volume of the Wigner-Seitz cell. The lattice energy density does not depend on the magnetic field, in accordance with the Bohr-van Leeuwen theorem [41]. For given P and B , the Gibbs energy (4) is computed for all possible A

¹ We neglect a small contribution from quantum zero-point motion of ions, which is typically a few orders of magnitude smaller than \mathcal{E}_L and its magnetic field dependence is known to be saturated [38]. Thus, we can safely neglect this term.

² B_e is parametrized as a function of Z as $B_e(Z) = 1.44381 \times 10^{-5} Z^{2.39} + 1.55468 \times 10^{-12} Z^{5.35}$, in units of MeV [39].

³ $C_M = 0.895929255682$ for a body-centered-cubic (BCC) lattice.

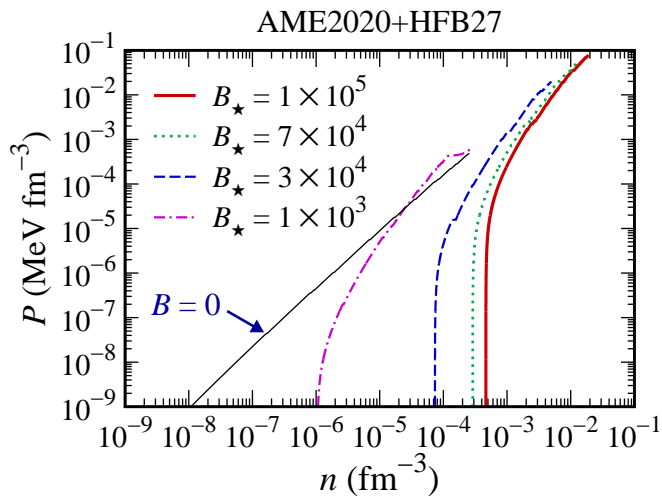


FIG. 2. Equations of state. Pressure P is plotted as a function of average nucleon number density n in the outer crust of strongly-magnetized neutron stars for representative magnetic field strengths.

and Z , and we regard the minimum one as the equilibrium composition. Thus, each layer of the outer crust is assumed to be composed of a single kind of nuclei forming a perfect BCC lattice, as in Refs. [24, 25].

Effects of a magnetic field on the equation of state (EoS).— Let us begin with discussion on the EoS, *i.e.* pressure P as a function of density n , for various magnetic field strengths; see Fig. 2. EoS for $B = 0$ is also exhibited by a solid line for comparison. From the figure, it is visible that the P - n curve drops more and more rapidly at a small n region, as the magnetic field strength increases. It is caused by the enhanced electron fraction due to the Landau-Rabi quantization of electron motion. Because of the charge neutrality condition, $n_p = n_e$, the crust composition is kept fixed, which makes the crustal matter almost incompressible, for a wide range of pressure. Note that the EoS lines end at high pressure and density, when a transition from the outer crust to the inner one occurs, *i.e.* neutrons start dripping out of nuclei. The neutron drip occurs when the neutron chemical potential exceeds its rest mass energy. Thus, we consider that the neutron drip occurs when the condition, $\min_{A,Z} [g(A, Z; P, B_*)] = \mu_n \geq m_n c^2$, is fulfilled, where the first equality follows from the β -equilibrium condition [42]. An important observation is that the neutron-drip pressure and density are significantly increased for $B_* \gtrsim 10^4$. For $B_* \gtrsim 10^4$, density goes well beyond $n_{\text{drip}}(B = 0) \approx 2.6 \times 10^{-4} \text{ fm}^{-3}$, which is never accessible for smaller magnetic field strengths. We have discovered really exotic nuclear species in this high density region.

The finding: Emergence of N -rich heavy and superheavy nuclei.— The resulting outer crust compositions obtained with various mass models are presented in Fig. 3 for representative magnetic field strengths. In the upper (lower) panels, the neutron (proton) number is shown as a function of density. The composition calculated without the magnetic field ($B = 0$) is also shown in (a) and (f) for comparison. For $B_* \lesssim 10^3$, nuclides that appear in the outer crust are not so much dependent on the magnetic field strength and the emerging atomic

number is, at most, $Z = 42$, consistent with earlier studies [24, 25]. In this region, the stabilization effects of neutron magic numbers $N = 50$ and 82 and that of protons $Z = 28$ are pronounced. In stark contrast, we find substantial dependence of the compositions on the magnetic field strength for $B_* \gtrsim 10^4$. At around $B_* = 3 \times 10^4$ [(c) and (h)], nuclei with $Z > 42$ emerge, which were absent for smaller B , where the next neutron magic number, $N = 126$, is reached at a bottom layer of the outer crust. At around $B_* = 7 \times 10^4$ [(d) and (i)], even more heavier nuclei $82 \lesssim Z \lesssim 92$ with $N = 184$ show up. The latter two neutron magic numbers, $N = 126$ and 184 with $54 \lesssim Z \lesssim 92$ have been overlooked in preceding studies [24, 25, 27].

It is not the end of the story. Interestingly enough, at around $B_* = 10^5$, the microscopic HFB-27 and HFB-32 mass models predict the existence of SHN with $Z > 104$ including the unknown elements, 119, 120, 122, and 124, with a significantly large neutron number $N \approx 260$ – 287 . Note that a naive counting of single-particle orbitals in a spherical Woods-Saxon potential with the spin-orbit coupling gives us $N = 258$ as the next magic number after $N = 184$. It explains a huge jump from $N = 184$ to 260 – 287 in the equilibrium compositions, observed in Fig. 1 and Fig. 3(e). Intriguingly, the BML mass model captures $N = 184$ magicity in the lead region, while the next magic number around $N = 258$ in the superheavy region is not encoded, resulting in smaller mass and atomic numbers for $B_* = 10^5$ as compared to those of HFB mass models. Though it is not clear in Fig. 3, but SHN do not appear for KTUY at $B_* = 10^5$. We have confirmed that SHN with $Z = 104, 106$, and 108 with $N = 184$ and 200 appear also for KTUY at a slightly larger B value, $B_* = 1.4 \times 10^5$. Thus, our results are quite robust, at least qualitatively, showing slight quantitative model dependence only in bottom layers of the outer crust, where very N -rich nuclei come into play. We point out that the maximum atomic number Z_{max} involved in the available theoretical mass tables depends on the models. For instance, Z_{max} is 124, 120, 132, and 130 for HFB-27 [6], HFB-32 [32], BML [33], and KTUY [34], respectively, while some other mass models do not include, *e.g.*, $Z > 110$ which limits applicability. We stress here that to obtain correct equilibrium compositions under a superstrong magnetic field, it is essential to include all possible A and Z , without any biased exclusion of mass and/or neutron numbers. (See Supplemental Material [42] for complete lists of the compositions.)

Discussion.—One may claim that the predicted magnetic field strength $B_* \gtrsim 10^5$ (*i.e.* $B \gtrsim 4 \times 10^{18}$ G) for the emergence of extremely N -rich SHN is too strong that is out of reach of existing magnetars. However, there exist theoretical arguments that allow existence of magnetars with $B \approx 10^{18}$ G [15–18], and the possibility should not be ruled out. Moreover, we expect that the effects of a magnetic field on nuclear structure, which has been neglected in this work, will strengthen the finding. Namely, in Ref. [24], fully self-consistent CDFT calculations were performed for Fe to Zn, showing that nuclear binding energy actually increases with the magnetic field strength and it becomes larger for higher

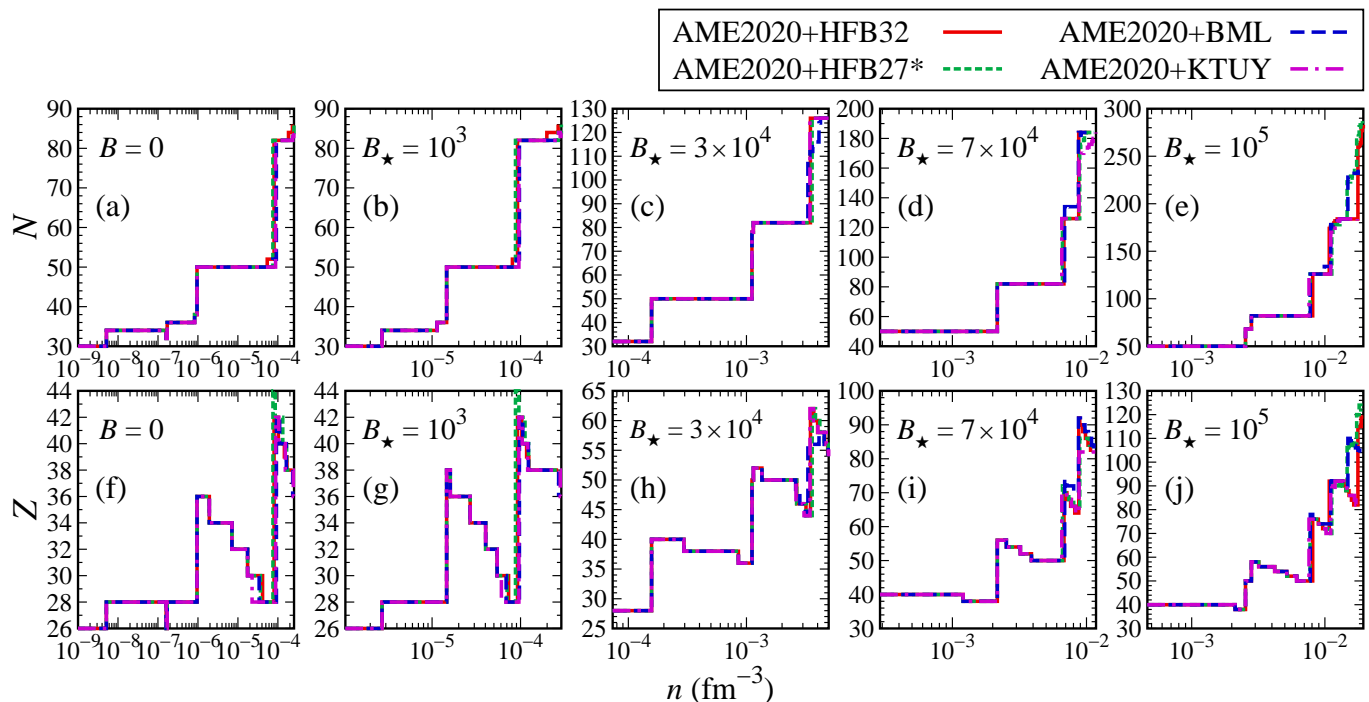


FIG. 3. The outer-crust compositions calculated with the latest experimental masses, AME2020 [7, 8], supplemented with various theoretical mass models (HFB-27 [6], HFB-32 [32], BML [33], and KTUY [34]) are shown for representative magnetic field strengths. In upper (lower) panels, the neutron (proton) number is shown as a function of average baryon (nucleon) number density n . From left to right panels, the magnetic field strength corresponds to: $B_\star = 0$ (*i.e.* without magnetic field), 10^3 (4.4×10^{16} G), 3×10^4 (1.3×10^{18} G), 7×10^4 (3.1×10^{18} G), and 10^5 (4.4×10^{18} G).

Z . We anticipate that if a strong magnetic field does stabilize SHN as well, they could emerge at lower magnetic field strengths than $B_\star \approx 10^5$, thus, it should be regarded as an upper bound for the critical magnetic field for the emergence of SHN.

We note, however, that the situation is not so obvious. First, nuclear mass models for the ground states involve effects of pairing correlations, which must vanish above a certain critical magnetic field ($B \gtrsim 10^{17}$ G) which breaks spin-singlet Cooper pairs [30]. Second, it is known that a magnetic field affects nuclear structure above $B \gtrsim 10^{17}$ G at which spin-dependent shifts of single-particle energy levels become on the order of MeV [23, 31]. When such shifts of energy levels change their ordering or shell structure, nuclear deformation as well as masses could be changed, which would affect the equilibrium composition. In addition, because of the different signs of the intrinsic magnetic moment of neutrons and protons ($g_n = -3.8263$ and $g_p = 5.5856$), time-odd currents rotate in opposite directions about the magnetic field axis [31]. The aforementioned effects are expected to be larger for heavier nuclei, because of the higher level density around the Fermi level and contributions of orbitals with larger angular momenta. To draw a quantitative conclusion, it is thus highly desired to extend the works of Refs. [23, 24, 31] based on microscopic self-consistent calculations to a wider mass region, including extremely N -rich SHN, under superstrong magnetic fields.

One may expect that the emergence of SHN may have a significant impact on the crustal properties. As prominent exam-

ples we present in Figs. 4(a) and 4(b), respectively, the effective shear modulus of the outer crust, $S = 0.1194 n_{\text{nucl}} Z^2 e^2 / R$ [25, 43], where $R = (3/4\pi n_N)^{1/3}$ is radius of the Wigner-Seitz cell, and the melting (or crystallizing) temperature, $T_{\text{melt}} = Z^2 e^2 / (k_B \Gamma R)$ [44], where k_B is the Boltzmann constant and $\Gamma = 175$ is the Coulomb coupling parameter at melting, as a function of pressure for representative magnetic field strengths. From the figure we find that both shear modulus and effective temperature increase dramatically with the magnetic field strength. It is associated with the increase of density n for a given pressure P , as shown in Fig. 2. The abrupt changes of S and T_{melt} as a function of P correspond to the change of the compositions, since they are in the strongly quantized regime (*i.e.* $\nu_{\text{max}} = 0$) for almost all pressure [42]. Because the neutron drip pressure substantially increases with the magnetic field strengths B , the maximum values of the effective shear modulus and the melting temperature increase with B . The orders of magnitude increase of the effective shear modulus implies that the outer crust of strongly-magnetized neutron stars is far more rigid than previously thought. It would bring new insight into physics of quasi-periodic oscillations (QPO), giant flares and starquakes, as well as a continuous gravitational wave emission from mountains at the surface [46], and so forth. Further, the substantial increase of the melting temperature may affect thermal evolution of strongly-magnetized proto-neutron stars. Since the changes of crustal properties are so large, they could have detectable consequences if such a strongly-magnetized neutron star is born.

Conclusions.—In this work, we have systematically inves-

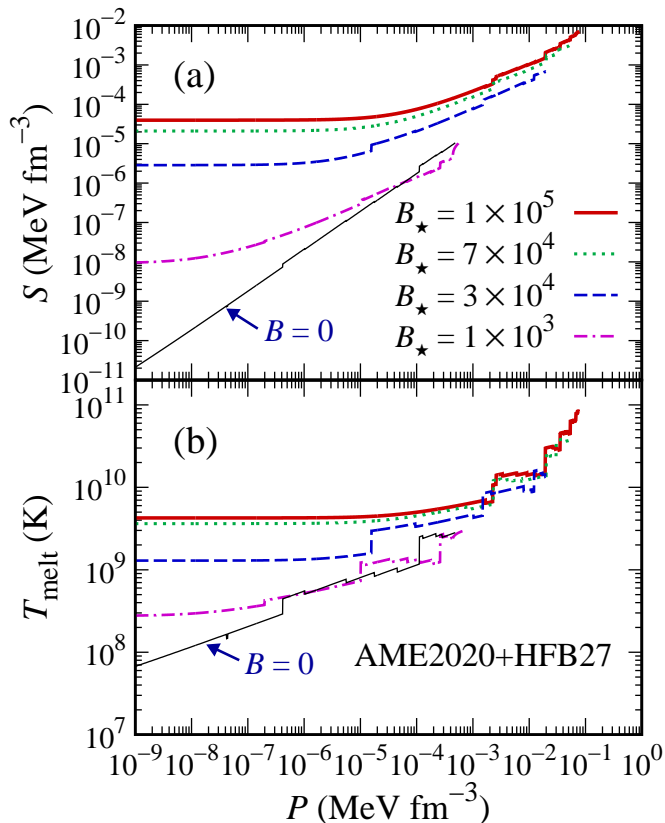


FIG. 4. (a) Effective shear modulus S and (b) melting temperature T_{melt} for the outer crust of strongly-magnetized neutron stars are shown as a function of pressure P for representative magnetic field strengths [45].

tigated outer crust compositions for a wide range of pressures (densities) and magnetic field strengths, adopting the latest experimental masses supplemented with various mass models. By exploring the optimal equilibrium composition of nuclei from the entire nuclear chart, we have found, for $B \gtrsim 10^{18}$ G, the emergence of neutron-rich heavy nuclei, which are much heavier than those found in preceding studies, showing a clear manifestation of neutron magic numbers, $N = 50, 82, 126$, as well as 184. Moreover, for $B \gtrsim 4 \times 10^{18}$ G, we have found that superheavy nuclei (SHN) with $Z \geq 104$ naturally emerge as equilibrium compositions that minimize the Gibbs energy. We have demonstrated that crustal properties, such as shear modulus and melting temperature, are dramatically increased by orders of magnitude by the magnetic field. As a consequence, *e.g.*, the breaking strain of the crust may become substantially larger than that without magnetic field effects. It results in a larger maximum ellipticity which may be detected as continuous gravitational waves from mountains at the neutron star surface, if such a superstrong magnetar exists. Such observations would imply the existence of SHN, giving important feedback to microscopic theories.

The finding will open a new exciting research area, building a bridge between studies of SHN and neutron stars, leaving a lot of open questions, *e.g.*: *i) Crustal properties of strongly-magnetized neutron stars.* Our calculations indicate that not

only the crust compositions, but also the crustal properties are substantially altered by the magnetic field. Its consequence, such as magnitude and frequency of crust oscillation modes, the maximum height of mountains and gravitational signals, thermal and electrical conductivities, as well as neutron star structure, should be reexamined. *ii) Effects of the magnetic field on nuclear structure.* In this work, we have found the emergence of extremely neutron-rich SHN with $N \approx 260\text{--}287$ for $B \gtrsim 4 \times 10^{18}$ G, while the magnetic field effects on nuclear structure were neglected. To draw a quantitative conclusion on the neutron and proton numbers of SHN and the critical magnetic field strength for their appearance, fully microscopic, self-consistent calculations are necessary for the entire nuclear chart, until the neutron drip line of SHN, for a wide range of magnetic field strengths. We mention here that in Ref. [47] axially-symmetric CDFT calculations were carried out including “hyperheavy” nuclei with $Z = 126\text{--}210$, where existence of toroidal nuclei has been advocated. Such calculations should also be achieved under superstrong magnetic fields to judge if they could exist in strongly-magnetized neutron stars. *iii) Properties of the inner crust.* For the strongest magnetic field neutrons start dripping out of SHN. Thus, the inner crust may also contain SHN under a superstrong magnetic field, before they transform into inhomogeneous crystalline structure (the so-called pasta phase [48]). In such a case, properties of dripped neutrons are most accurately described with the band theory of solids (see, Refs. [49–51], and references therein) which has never been applied taking into account the magnetic field effects. How structure and properties of the inner crust are affected by our finding is also an open question.

We are grateful Stephane Goriely for providing all the HFB mass tables currently available (from HFB-01 to HFB-32), which were useful to conduct this study. We are also thankful to Kei Iida and Takashi Nakatsukasa for providing useful comments on this Letter.

* sekizawa@phys.titech.ac.jp

- [1] S. Hofmann and G. Muenzenberg, The discovery of the heaviest elements, *Rev. Mod. Phys.* **72**, 733 (2000).
- [2] P. Armbruster, On the Production of Superheavy Elements, *Ann. Rev. Part. Sci.* **50**, 411 (2000).
- [3] J.H. Hamilton, S. Hofmann, and Y.T. Oganessian, Search for Superheavy Nuclei, *Ann. Rev. Part. Sci.* **63**, 383 (2013).
- [4] Y.T. Oganessian, A. Sobczewski, and G.M. Ter-Akopian, Superheavy nuclei: from predictions to discovery, *Phys. Scr.* **92**, 023003 (2017).
- [5] Colloquium: Superheavy elements: Oganessian and beyond, S.A. Giuliani, Z. Matheson, W. Nazarewicz, E. Olsen, P.-G. Reinhard, J. Sadhukhan, B. Schuetrumpf, N. Schunck, and P. Schwerdtfeger, *Rev. Mod. Phys.* **91**, 011001 (2019).
- [6] S. Goriely, N. Chamel, and J.M. Pearson, Hartree-Fock-Bogoliubov nuclear mass model with 0.50 MeV accuracy based on standard forms of Skyrme and pairing functionals, *Phys. Rev. C* **88**, 061302(R) (2013).
- [7] W.J. Huang, M. Wang, F.G. Kondev, G. Audi, and S. Naimi,

- The AME 2020 atomic mass evaluation (I). Evaluation of input data, and adjustment procedures, *Chinese Phys. C* **45**, 030002 (2021).
- [8] M. Wang, W.J. Huang, F.G. Kondev, G. Audi, and S. Naimi, The AME 2020 atomic mass evaluation (II). Tables, graphs and references, *Chinese Phys. C* **45**, 030003 (2021).
- [9] P. Haensel, A.Y. Potekhin, and D.G. Yakovlev, *Neutron Stars 1: Equation of State and Structure* (Springer, New York, 2007).
- [10] J.H. Seiradakis and R. Wielebinski, Morphology and characteristics of radio pulsars, *Astron. Astrophys. Rev.* **12**, 239 (2004).
- [11] C.-Y. Ng and V.M. Kaspi, High Magnetic Field Rotation Powered Pulsars, *AIP Conf. Proc.* **1379**, 60 (2011).
- [12] S. Mereghetti, The strongest cosmic magnets: soft gamma-ray repeaters and anomalous X-ray pulsars, *Astron. Astrophys. Rev.* **15**, 225 (2008).
- [13] S.A. Olausen and V.M. Kaspi, THE MCGILL MAGNETAR CATALOG, *Astrophys. J., Suppl. Ser.* **212**, 6 (2014).
- [14] A. Tiengo, P. Esposito, S. Mereghetti, R. Turolla, L. Nobili, F. Gastaldello, D. Götz, G.L. Israel, N. Rea, L. Stella, S. Zane, and G.F. Bignami, A variable absorption feature in the X-ray spectrum of a magnetar, *Nature (London)* **500**, 312 (2013).
- [15] A.Y. Potekhin, and D.G. Yakovlev, Electron conduction along quantizing magnetic fields in neutron star crusts II. Practical formulae, *Astron. Astrophys.* **314**, 341 (1996); Erratum: *ibid.* **327**, 442 (1997).
- [16] A.Y. Potekhin, Electron conduction in magnetized neutron star envelopes, *Astron. Astrophys.* **351**, 787 (1999).
- [17] A. Broderick, M. Prakash, and J.M. Lattimer, The Equation of State of Neutron Star Matter in Strong Magnetic Fields, *Astrophys. J.* **537**, 351 (2000).
- [18] J. Ventura and A.Y. Potekhin, Neutron Star Envelopes and Thermal Radiation from the Magnetic Surface, The Neutron Star-Black Hole Connection, in Proceedings of the NATO Advanced Study Institute, Elounda, Crete, Greece, June 7-18, 1999, NATO Science Series C, Vol. **567**, edited by C. Kouveliotou, J.E. Ventura, and E.P. van den Heuvel (Springer, Netherlands, 2001), pp. 393-414.
- [19] I. Fushiki, E.H. Gudmundsson, and C.J. Pethick, Surface structure of neutron stars with high magnetic fields, *Astrophys. J.* **342**, 958 (1989).
- [20] D. Lai and S.L. Shapiro, Cold equation of state in a strong magnetic field: Effects of inverse β -decay, *Astrophys. J.* **383**, 745 (1991).
- [21] V.N. Kondratyev, T. Maruyama, and S. Chiba, Shell Structure of Nuclei in Strong Magnetic Fields in Neutron Star Crusts, *Phys. Rev. Lett.* **84**, 1086 (2000).
- [22] V.N. Kondratyev, T. Maruyama, and S. Chiba, *Astrophys. J.* **546**, 1137 (2001).
- [23] D. Peña Arteaga, M. Grasso, E. Khan, and P. Ring, Nuclear structure in strong magnetic fields: Nuclei in the crust of a magnetar, *Phys. Rev. C* **84**, 045806 (2011).
- [24] D. Basilico, D.P. Arteaga, X. Roca-Maza, and G. Colò, Outer crust of a cold non-accreting magnetar, *Phys. Rev. C* **92**, 035802 (2015).
- [25] N. Chamel, R.L. Pavlov, L.M. Mihailov, Ch.J. Velchev, Zh.K. Stoyanov, Y.D. Mutafchieva, M.D. Ivanovich, J.M. Pearson, and S. Goriely, Properties of the outer crust of strongly magnetized neutron stars from Hartree-Fock-Bogoliubov atomic mass models, *Phys. Rev. C* **86**, 055804 (2012).
- [26] N. Chamel and Zh.K. Stoyanov, Analytical determination of the structure of the outer crust of a cold nonaccreted neutron star: Extension to strongly quantizing magnetic fields, *Phys. Rev. C* **101**, 065802 (2020).
- [27] V. Parmar, H.C. Das, M.K. Sharma, and S.K. Patra, Magnetized neutron star crust within effective relativistic mean-field model, arXiv:2211.07339v1 [astro-ph.HE].
- [28] I.I. Rabi, Das freie Elektron im homogenen Magnetfeld nach der Diracschen Theorie, *Z. Physik* **49**, 507 (1928).
- [29] L. Landau, Diamagnetismus der Metalle, *Z. Physik* **64**, 629 (1930).
- [30] M. Stein, A. Sedrakian, X.-G. Huang, and J.W. Clark, Spin-polarized neutron matter: Critical unpairing and BCS-BEC precursor, *Phys. Rev. C* **93**, 015802 (2016).
- [31] M. Stein, J. Maruhn, and A. Sedrakian, Carbon-oxygen-neon mass nuclei in superstrong magnetic fields, *Phys. Rev. C* **94**, 035802 (2016).
- [32] S. Goriely, N. Chamel, and J.M. Pearson, Further explorations of Skyrme-Hartree-Fock-Bogoliubov mass formulas. XVI. Inclusion of self-energy effects in pairing, *Phys. Rev. C* **93**, 034337 (2016).
- [33] Z.M. Niu and H.Z. Liang, Nuclear mass predictions with machine learning reaching the accuracy required by r-process studies, *Phys. Rev. C* **106**, L021303 (2022).
- [34] H. Koura, T. Tachibana, M. Uno, and M. Yamada, Nuclidic Mass Formula on a Spherical Basis with an Improved Even-Odd Term, *Prog. Theor. Phys.* **113**, 305 (2005).
- [35] K. Iida and T. Fujie, On the Stability of Giant Nuclei in Supernova Matter with Respect to Deconfinement, *JPS Conf. Proc.* **31**, 011057 (2020).
- [36] S. Aggarwal, B. Mukhopadhyay, and G. Gregori, Relativistic Landau quantization in non-uniform magnetic field and its applications to white dwarfs and quantum information, *SciPost Phys.* **11**, 093 (2021).
- [37] G. Baym, C. Pethick, and P. Sutherland, The ground state of matter at high densities: Equation of state and stellar models, *Astrophys. J.* **170**, 299 (1971).
- [38] D.A. Baiko, Coulomb crystals in the magnetic field, *Phys. Rev. E* **80**, 046405 (2009).
- [39] D. Lunney, J.M. Pearson, and C. Thibault, Recent trends in the determination of nuclear masses, *Rev. Mod. Phys.* **75**, 1021 (2003).
- [40] D.A. Baiko, A.Y. Potekhin, and D.G. Yakovlev, Thermodynamic functions of harmonic Coulomb crystals, *Phys. Rev. E* **64**, 057402 (2001).
- [41] J.H. Van Vleck, *The Theory of Electric and Magnetic Susceptibilities* (Oxford University Press, London, 1932).
- [42] See Supplemental Material at {URL will be provided by the publisher} for complete lists of the outer crust compositions and complementally figures.
- [43] S. Ogata and S. Ichimaru, First-principles calculations of shear moduli for Monte Carlo-simulated Coulomb solids, *Phys. Rev. A* **42**, 4867 (1990).
- [44] A.F. Fantina, S. De Ridder, N. Chamel, and F. Gulminelli, Crystallization of the outer crust of a non-accreting neutron star, *A&A* **633**, A149 (2020).
- [45] We note that the effective shear modulus S in Fig. 5 of Ref. [25] contains some error. We have confirmed that their results agree with ours with $B_\star = 0$ and 1.4×10^3 for $P \leq 8 \times 10^{-4} \text{ MeV fm}^{-3}$, after some correction. (N. Chamel, Private communications.)
- [46] C.J. Horowitz and K. Kadau, Breaking Strain of Neutron Star Crust and Gravitational Waves, *Phys. Rev. Lett.* **102**, 191102 (2009).
- [47] S.E. Agbemava and A.V. Afanasjev, Hyperheavy spherical and toroidal nuclei: The role of shell structure, *Phys. Rev. C* **103**, 034323 (2021).
- [48] M.E. Caplan and C.J. Horowitz, Colloquium: Astromaterial science and nuclear pasta, *Rev. Mod. Phys.* **89**, 041002 (2017).

- [49] N. Chamel, Entrainment in Superfluid Neutron-Star Crusts: Hydrodynamic Description and Microscopic Origin, *J. Low Temp. Phys.* **189**, 328 (2017).
- [50] Y. Kashiwaba and T. Nakatsukasa, Self-consistent band calculation of the slab phase in the neutron-star crust, *Phys. Rev. C* **100**, 035804 (2019).
- [51] K. Sekizawa, S. Kobayashi, and M. Matsuo, Time-dependent extension of the self-consistent band theory for neutron star matter: Anti-entrainment effects in the slab phase, *Phys. Rev. C* **105**, 045807 (2022).

Supplemental Online Material for: Possible Existence of Extremely Neutron-Rich Superheavy Nuclei in Neutron Star Crusts Under a Superstrong Magnetic Field

Kazuyuki Sekizawa^{1,2,*} and Kentaro Kaba¹

¹*Department of Physics, School of Science, Tokyo Institute of Technology, Tokyo 152-8551, Japan*

²*Nuclear Physics Division, Center for Computational Sciences, University of Tsukuba, Ibaraki 305-8577, Japan*

³*RIKEN Nishina Center, Saitama 351-0198, Japan*

In this Supplemental Material, we provide supplementary explanations that may help to understand the effects of strong magnetic fields on the outer crust compositions, the main results of the paper. We also present numerical tables showing various quantities obtained with four mass models used (HFB-27, HFB-32, BML, and KTUY) for a full range of pressures (densities) and magnetic field strengths.

On the neutron drip

By definition, there follows a thermodynamic relation,

$$G \equiv gn = \mu_n n_n + \mu_p n_p + \mu_e n_e, \quad (5)$$

where G denotes the Gibbs energy (g is the Gibbs energy per nucleon), n is the average baryon (nucleon) number density, μ_i and n_i are the chemical potential and the average number density of particle i ($= n, p, \text{ or } e$), respectively. Because of the charge neutrality condition, $n_p = n_e$, and the β -equilibrium condition, $\mu_n = \mu_p + \mu_e$, the right hand side of Eq. (5) can be written as

$$G = \mu_n n. \quad (6)$$

It means that the chemical potential of neutrons is equal to the Gibbs energy per nucleon, *i.e.* $\mu_n = g$, that is, the neutron drip pressure P_{drip} is defined by the condition, $g(P_{\text{drip}}) = \mu_n = m_n c^2$. We thus performed calculations until the condition,

$$\min_{A,Z} [g(A, Z; P, B)] \geq m_n c^2, \quad (7)$$

is fulfilled for all sets of the mass and atomic numbers (A, Z).

In Figs. 5(a) and 5(b), we show the resulting neutron drip pressure and density, P_{drip} and n_{drip} , respectively, as a function of the magnetic field strength $B_\star = B/B_c$ with $B_c \simeq 4.41 \times 10^{13}$ G. From the figure, we see that P_{drip} and n_{drip} are almost independent from the mass models used. Also, it is visible that P_{drip} and n_{drip} are hardly affected for $B_\star \lesssim 10^3$. As the magnetic field strength increases, P_{drip} and n_{drip} start increasing nearly linearly for $B_\star \gtrsim 10^3$. A kink in between $B_\star = 1000$ and 2000 is associated with a transition to the strongly-quantizing regime where $\nu_{\text{max}} = 1 \rightarrow 0$ takes place. The observed increase of the neutron drip density is the key to pave a way to the region where very neutron-rich heavy and superheavy nuclei emerge, as we discussed in the main texts.

On the electron fraction

It is important to understand why the electron fraction is suppressed due to the presence of a strong magnetic field. To

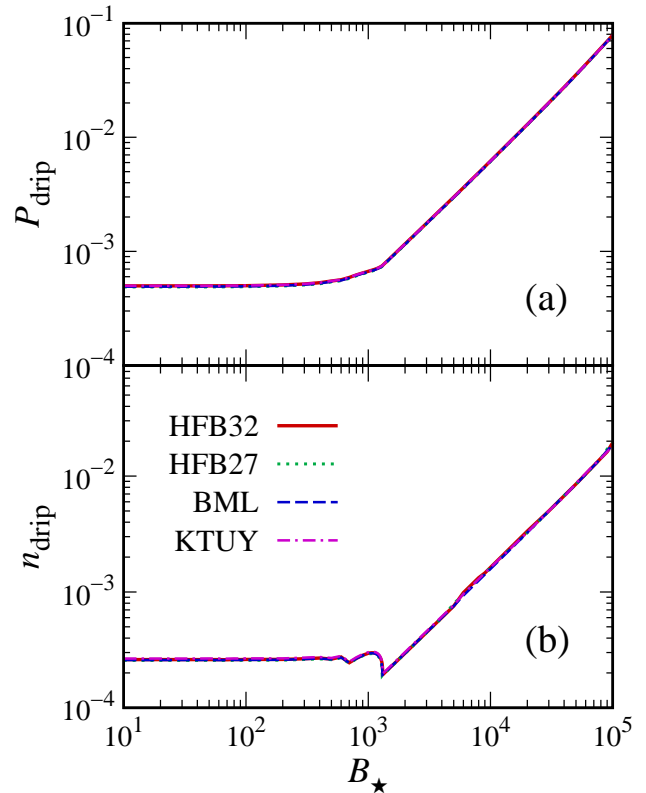


FIG. 5. (a) Neutron-drip pressure P_{drip} and (b) density n_{drip} for strongly-magnetized neutron stars are shown as a function of the magnetic field strength $B_\star = B/B_c$ with $B_c \simeq 4.41 \times 10^{13}$ G.

see this, let us consider the strongly-quantizing regime where only the lowest Landau level is occupied, *i.e.* $\nu_{\text{max}} = 0$. In this case, the expression for the electron number density (2) is reduced to

$$n_e = \frac{2B_\star}{(2\pi)^2 \lambda_e^3} \sqrt{\frac{\mu_e}{m_e c^2} - 1}. \quad (8)$$

It is apparent that the electron number density n_e is proportional to the magnetic field strength, leading to enhancement of the electron fraction. Thus, for a given pressure P , which has corresponding density n , the proton number density is enhanced via the charge neutrality condition, $n_p = n_e$, resulting

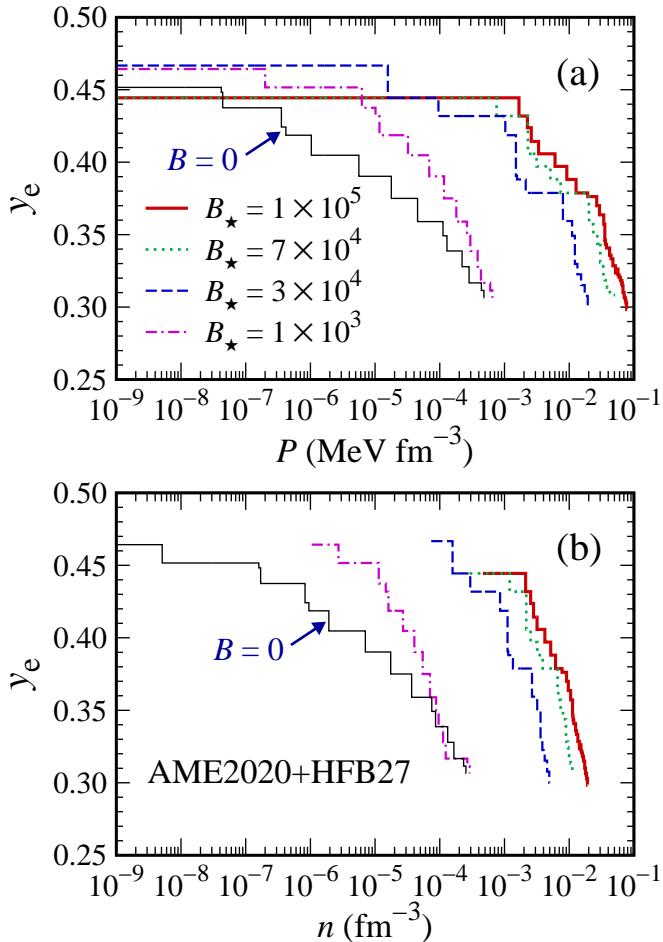


FIG. 6. Electron fraction $y_e = Z/A$ in the outer crust of strongly-magnetized neutron stars is shown as a function of pressure (a) and density (b) for representative magnetic field strengths.

in the reduction of neutron richness.

In Fig. 6(a), we show the calculated electron fraction $y_e = Z/A$ as a function of pressure P for representative magnetic field strengths. The case without magnetic field (*i.e.* $B=0$) is also shown for comparison. A larger electron fraction indicates a larger proton fraction and, thus, a less neutron-rich composition. By comparing the results for $B=0$ (thin solid line) with $B_* = 10^3$ (dashed line) and 3×10^4 (dash-dotted line) for $P < P_{\text{drip}}(B=0)$, one finds an enhancement of the electron fraction due to the presence of the magnetic field. On the other hand, we find that y_e is actually smaller for $B_* = 7 \times 10^4$ (dotted line) and 10^5 (solid line) as compared to the $B=0$ case for $P \lesssim 4 \times 10^{-8}$. It is because of the fact that density n is much higher under such strong magnetic fields, see Fig. 6(b). In the figure, the same results are plotted as in Fig. 6(a), but the horizontal axis is replaced with density n . Because of the higher density, neutron-rich heavy nuclei with larger neutron magic numbers $N = 50$ and 126 emerge, explaining a bit smaller value of y_e for $P \lesssim 4 \times 10^{-8}$. As is evident from Fig. 6(b), for $B_* \gtrsim 10^4$ density can reach much higher values than $n_{\text{drip}}(B=0)$, where really exotic nuclei, including extremely neutron-rich superheavy nuclei, emerge.

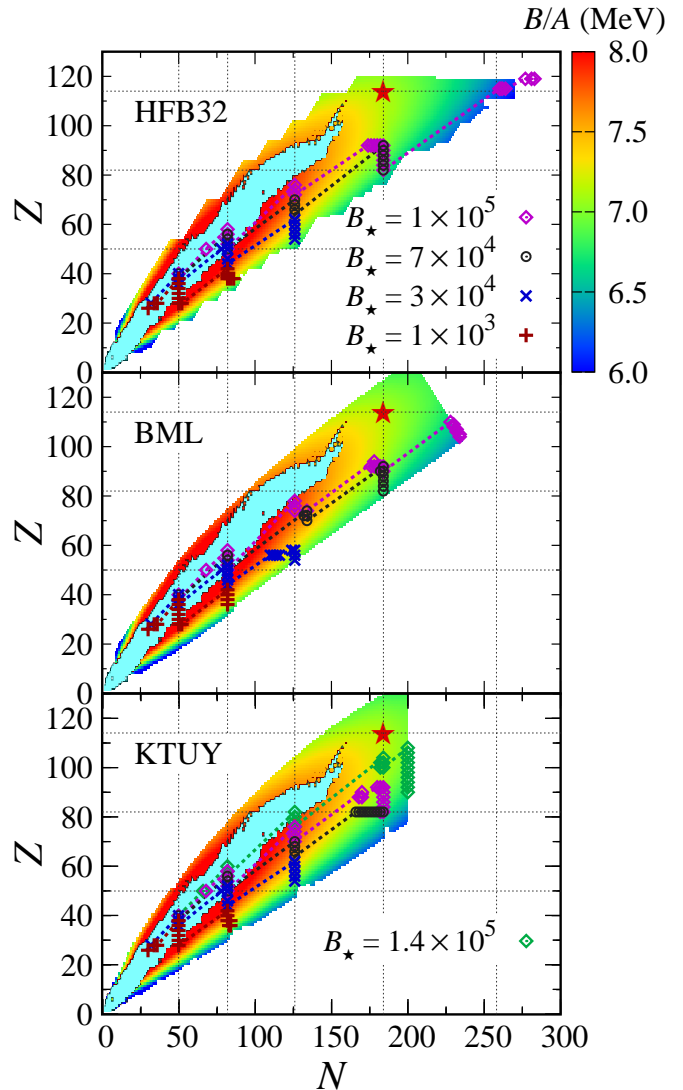


FIG. 7. Same as Fig. 1 (in the main texts), but calculated with other theoretical mass models, HFB-32 [32] (top), BML [33], and KTUY [34]. For the results with the KTUY mass model, those for $B_* = 1.4 \times 10^5$ are also shown, for which emergence of superheavy nuclei $Z = 104, 106$ and 108 are observed.

Crust compositions

For completeness, we show in Fig. 7 the outer crust compositions calculated with the latest experimental masses, AME2020 [7, 8], supplemented with different mass models, HFB-32 [32] (top), BML [33] (middle), and KTUY [34] (bottom). From Figs. 1 and 7, we find that the microscopic HFB mass models predicts a substantial stabilization effect around $N = 258$ in the superheavy region, whereas it is absent in the BML and KTUY mass models. Apparently, BML and KTUY suffer from limited neutron numbers included in the mass table. It is thus important to provide mass tables up to $Z \approx 130$ or beyond, until the drip lines.

Numerical tables

Below we provide numerical tables obtained in this study.

TABLE I. The results of BPS model calculations for $B = 0$ with the experimental masses, AME2020 [7, 8], supplemented with the microscopic mass model, HFB-27 [6]. In the first to fourth columns, the outer crust composition [*i.e.*, nuclides, ${}^A\text{X}$, where X stands for the corresponding symbol of the element, proton, neutron, and mass numbers, Z, N, A , are presented, respectively. In the fifth to sixth columns, the corresponding electron fraction, $y_e = Z/A$, and N/Z ratio are shown, respectively. In the seventh (eighth) column, the maximum density n_{max} (pressure P_{max}) are given in units of fm^{-3} (MeV fm^{-3}), below which the corresponding nuclide exists. From the ninth to eleventh columns, it shows: $R = (3/4\pi n_N)^{1/3}$, the radius of the Wigner-Seitz cell in units of fm, $\hbar\omega_p$, energy of the plasma oscillation in units of MeV, and $S = 0.1194n_N Z^2 e^2/R$, the effective shear modulus in units of MeV fm^{-3} , respectively.

AME2020+HFB27 ($B = 0$)										
Nuclides	Z	N	A	y_e	N/Z	$n_{\text{max}} [\text{fm}^{-3}]$	$P_{\text{max}} [\text{MeV}/\text{fm}^3]$	$R [\text{fm}]$	$\hbar\omega [\text{MeV}]$	$S [\text{MeV}/\text{fm}^3]$
${}^{56}\text{Fe}$	26	30	56	0.46	1.15	4.94×10^{-9}	3.37×10^{-10}	1.39×10^3	8.98×10^{-4}	7.35×10^{-12}
${}^{62}\text{Ni}$	28	34	62	0.45	1.21	1.58×10^{-7}	4.16×10^{-8}	4.54×10^2	4.94×10^{-3}	7.55×10^{-10}
${}^{58}\text{Fe}$	26	32	58	0.45	1.23	1.65×10^{-7}	4.37×10^{-8}	4.38×10^2	5.01×10^{-3}	7.53×10^{-10}
${}^{64}\text{Ni}$	28	36	64	0.44	1.29	7.96×10^{-7}	3.53×10^{-7}	2.68×10^2	1.07×10^{-2}	6.25×10^{-9}
${}^{66}\text{Ni}$	28	38	66	0.42	1.36	9.24×10^{-7}	4.14×10^{-7}	2.57×10^2	1.12×10^{-2}	7.33×10^{-9}
${}^{86}\text{Kr}$	36	50	86	0.42	1.39	1.85×10^{-6}	1.02×10^{-6}	2.23×10^2	1.57×10^{-2}	2.15×10^{-8}
${}^{84}\text{Se}$	34	50	84	0.40	1.47	6.77×10^{-6}	5.56×10^{-6}	1.43×10^2	2.90×10^{-2}	1.11×10^{-7}
${}^{82}\text{Ge}$	32	50	82	0.39	1.56	1.67×10^{-5}	1.76×10^{-5}	1.05×10^2	4.38×10^{-2}	3.39×10^{-7}
${}^{80}\text{Zn}$	30	50	80	0.38	1.67	3.49×10^{-5}	4.49×10^{-5}	8.18×10^1	6.09×10^{-2}	8.24×10^{-7}
${}^{78}\text{Ni}$	28	50	78	0.36	1.79	7.17×10^{-5}	1.11×10^{-4}	6.38×10^1	8.36×10^{-2}	1.94×10^{-6}
${}^{126}\text{Ru}$	44	82	126	0.35	1.86	8.28×10^{-5}	1.28×10^{-4}	7.13×10^1	8.74×10^{-2}	3.06×10^{-6}
${}^{124}\text{Mo}$	42	82	124	0.34	1.95	1.27×10^{-4}	2.19×10^{-4}	6.15×10^1	1.05×10^{-1}	5.07×10^{-6}
${}^{122}\text{Zr}$	40	82	122	0.33	2.05	1.58×10^{-4}	2.80×10^{-4}	5.68×10^1	1.14×10^{-1}	6.28×10^{-6}
${}^{120}\text{Sr}$	38	82	120	0.32	2.16	2.27×10^{-4}	4.34×10^{-4}	5.01×10^1	1.31×10^{-1}	9.39×10^{-6}
${}^{122}\text{Sr}$	38	84	122	0.31	2.21	2.47×10^{-4}	4.75×10^{-4}	4.90×10^1	1.35×10^{-1}	1.03×10^{-5}
${}^{124}\text{Sr}$	38	86	124	0.31	2.26	2.55×10^{-4}	4.84×10^{-4}	4.88×10^1	1.35×10^{-1}	1.05×10^{-5}

TABLE II. Same as Table I, but for $B_* = 10^3$. Here and also in the tables below, the highest occupied Landau level ν_{max} is also shown for $B \neq 0$ cases.

AME2020+HFB27 ($B_* = 10^3$)											
Nuclides	Z	N	A	y_e	N/Z	$n_{\text{max}} [\text{fm}^{-3}]$	$P_{\text{max}} [\text{MeV}/\text{fm}^3]$	ν_{max}	$R [\text{fm}]$	$\hbar\omega [\text{MeV}]$	$S [\text{MeV}/\text{fm}^3]$
${}^{56}\text{Fe}$	26	30	56	0.46	1.15	2.62×10^{-6}	1.97×10^{-7}	0	1.72×10^2	2.07×10^{-2}	3.16×10^{-8}
${}^{62}\text{Ni}$	28	34	62	0.45	1.21	1.10×10^{-5}	6.18×10^{-6}	0	1.10×10^2	4.12×10^{-2}	2.16×10^{-7}
${}^{64}\text{Ni}$	28	36	64	0.44	1.29	1.42×10^{-5}	1.01×10^{-5}	0	1.02×10^2	4.54×10^{-2}	2.93×10^{-7}
${}^{88}\text{Sr}$	38	50	88	0.43	1.32	1.55×10^{-5}	1.16×10^{-5}	0	1.11×10^2	4.68×10^{-2}	3.96×10^{-7}
${}^{86}\text{Kr}$	36	50	86	0.42	1.39	2.60×10^{-5}	3.19×10^{-5}	0	9.25×10^1	5.87×10^{-2}	7.28×10^{-7}
${}^{84}\text{Se}$	34	50	84	0.40	1.47	3.88×10^{-5}	6.79×10^{-5}	0	8.03×10^1	6.93×10^{-2}	1.14×10^{-6}
${}^{82}\text{Ge}$	32	50	82	0.39	1.56	5.20×10^{-5}	1.15×10^{-4}	0	7.22×10^1	7.75×10^{-2}	1.55×10^{-6}
${}^{80}\text{Zn}$	30	50	80	0.38	1.67	6.71×10^{-5}	1.78×10^{-4}	0	6.58×10^1	8.45×10^{-2}	1.97×10^{-6}
${}^{78}\text{Ni}$	28	50	78	0.36	1.79	8.45×10^{-5}	2.60×10^{-4}	0	6.04×10^1	9.08×10^{-2}	2.42×10^{-6}
${}^{126}\text{Ru}$	44	82	126	0.35	1.86	9.25×10^{-5}	2.93×10^{-4}	0	6.88×10^1	9.24×10^{-2}	3.55×10^{-6}
${}^{124}\text{Mo}$	42	82	124	0.34	1.95	1.08×10^{-4}	3.80×10^{-4}	0	6.49×10^1	9.70×10^{-2}	4.08×10^{-6}
${}^{122}\text{Zr}$	40	82	122	0.33	2.05	1.19×10^{-4}	4.28×10^{-4}	0	6.26×10^1	9.82×10^{-2}	4.27×10^{-6}
${}^{120}\text{Sr}$	38	82	120	0.32	2.16	2.60×10^{-4}	5.94×10^{-4}	0, 1	4.79×10^1	1.40×10^{-1}	1.12×10^{-5}
${}^{122}\text{Sr}$	38	84	122	0.31	2.21	2.82×10^{-4}	6.44×10^{-4}	1	4.69×10^1	1.44×10^{-1}	1.23×10^{-5}
${}^{124}\text{Sr}$	38	86	124	0.31	2.26	2.89×10^{-4}	6.50×10^{-4}	1	4.68×10^1	1.43×10^{-1}	1.24×10^{-5}

TABLE III. Same as Tables I and II, but for $B_* = 3 \times 10^4$.

AME2020 + HFB27 ($B_* = 3 \times 10^4$)											
Nuclides	Z	N	A	y_e	N/Z	$n_{\max} [\text{fm}^{-3}]$	$P_{\max} [\text{MeV}/\text{fm}^3]$	ν_{\max}	$R [\text{fm}]$	$\hbar\omega [\text{MeV}]$	$S [\text{MeV}/\text{fm}^3]$
⁶⁰ Ni	28	32	60	0.47	1.14	1.37×10^{-4}	1.56×10^{-5}	0	4.71×10^1	1.50×10^{-1}	6.54×10^{-6}
⁹⁰ Zr	40	50	90	0.44	1.25	2.88×10^{-4}	9.43×10^{-5}	0	4.21×10^1	2.08×10^{-1}	2.09×10^{-5}
⁸⁸ Sr	38	50	88	0.43	1.32	8.27×10^{-4}	1.02×10^{-3}	0	2.94×10^1	3.42×10^{-1}	7.94×10^{-5}
⁸⁶ Kr	36	50	86	0.42	1.39	1.01×10^{-3}	1.48×10^{-3}	0	2.73×10^1	3.67×10^{-1}	9.65×10^{-5}
¹²⁸ Sn	50	78	128	0.39	1.56	1.13×10^{-3}	1.54×10^{-3}	0	3.00×10^1	3.61×10^{-1}	1.26×10^{-4}
¹³⁴ Te	52	82	134	0.39	1.58	1.31×10^{-3}	2.10×10^{-3}	0	2.90×10^1	3.87×10^{-1}	1.57×10^{-4}
¹³² Sn	50	82	132	0.38	1.64	2.52×10^{-3}	7.90×10^{-3}	0	2.32×10^1	5.23×10^{-1}	3.53×10^{-4}
¹²⁸ Pd	46	82	128	0.36	1.78	3.10×10^{-3}	1.10×10^{-2}	0	2.14×10^1	5.51×10^{-1}	4.11×10^{-4}
¹²⁶ Ru	44	82	126	0.35	1.86	3.35×10^{-3}	1.21×10^{-2}	0	2.08×10^1	5.56×10^{-1}	4.25×10^{-4}
¹⁸⁸ Sm	62	126	188	0.33	2.03	3.74×10^{-3}	1.33×10^{-2}	0	2.29×10^1	5.54×10^{-1}	5.74×10^{-4}
¹⁸⁶ Nd	60	126	186	0.32	2.10	4.06×10^{-3}	1.51×10^{-2}	0	2.22×10^1	5.65×10^{-1}	6.09×10^{-4}
¹⁸⁴ Ce	58	126	184	0.32	2.17	4.42×10^{-3}	1.72×10^{-2}	0	2.15×10^1	5.76×10^{-1}	6.47×10^{-4}
¹⁸² Ba	56	126	182	0.31	2.25	4.77×10^{-3}	1.92×10^{-2}	0	2.09×10^1	5.84×10^{-1}	6.77×10^{-4}
¹⁸⁰ Xe	54	126	180	0.30	2.33	4.96×10^{-3}	1.97×10^{-2}	0	2.05×10^1	5.81×10^{-1}	6.73×10^{-4}

TABLE IV. Same as Tables I-III, but for $B_* = 7 \times 10^4$.

AME2020 + HFB27 ($B_* = 7 \times 10^4$)											
Nuclides	Z	N	A	y_e	N/Z	$n_{\max} [\text{fm}^{-3}]$	$P_{\max} [\text{MeV}/\text{fm}^3]$	ν_{\max}	$R [\text{fm}]$	$\hbar\omega [\text{MeV}]$	$S [\text{MeV}/\text{fm}^3]$
⁹⁰ Zr	40	50	90	0.44	1.25	1.17×10^{-3}	7.47×10^{-4}	0	2.64×10^1	4.18×10^{-1}	1.36×10^{-4}
⁸⁸ Sr	38	50	88	0.43	1.32	1.95×10^{-3}	2.28×10^{-3}	0	2.21×10^1	5.25×10^{-1}	2.49×10^{-4}
¹³⁸ Ba	56	82	138	0.41	1.46	2.47×10^{-3}	3.10×10^{-3}	0	2.37×10^1	5.55×10^{-1}	4.07×10^{-4}
¹³⁶ Xe	54	82	136	0.40	1.52	3.13×10^{-3}	5.05×10^{-3}	0	2.18×10^1	6.12×10^{-1}	5.30×10^{-4}
¹³⁴ Te	52	82	134	0.39	1.58	3.79×10^{-3}	7.30×10^{-3}	0	2.04×10^1	6.57×10^{-1}	6.45×10^{-4}
¹³² Sn	50	82	132	0.38	1.64	6.21×10^{-3}	1.99×10^{-2}	0	1.72×10^1	8.21×10^{-1}	1.18×10^{-3}
¹⁹⁸ Hf	72	126	198	0.36	1.75	6.62×10^{-3}	2.01×10^{-2}	0	1.93×10^1	8.14×10^{-1}	1.55×10^{-3}
¹⁹⁶ Yb	70	126	196	0.36	1.80	7.22×10^{-3}	2.34×10^{-2}	0	1.86×10^1	8.35×10^{-1}	1.67×10^{-3}
¹⁹⁴ Er	68	126	194	0.35	1.85	7.85×10^{-3}	2.69×10^{-2}	0	1.81×10^1	8.54×10^{-1}	1.78×10^{-3}
¹⁹² Dy	66	126	192	0.34	1.91	8.41×10^{-3}	3.00×10^{-2}	0	1.76×10^1	8.67×10^{-1}	1.86×10^{-3}
²⁶⁰ Rn	86	174	260	0.33	2.02	8.95×10^{-3}	3.06×10^{-2}	0	1.91×10^1	8.61×10^{-1}	2.30×10^{-3}
²⁶² Rn	86	176	262	0.33	2.05	9.37×10^{-3}	3.31×10^{-2}	0	1.88×10^1	8.73×10^{-1}	2.41×10^{-3}
²⁶⁵ Rn	86	179	265	0.32	2.08	9.52×10^{-3}	3.34×10^{-2}	0	1.88×10^1	8.70×10^{-1}	2.43×10^{-3}
²⁶⁸ Rn	86	182	268	0.32	2.12	9.85×10^{-3}	3.51×10^{-2}	0	1.86×10^1	8.76×10^{-1}	2.51×10^{-3}
²⁷⁰ Rn	86	184	270	0.32	2.14	1.03×10^{-2}	3.81×10^{-2}	0	1.84×10^1	8.89×10^{-1}	2.63×10^{-3}
²⁶⁸ Po	84	184	268	0.31	2.19	1.10×10^{-2}	4.20×10^{-2}	0	1.80×10^1	9.02×10^{-1}	2.76×10^{-3}
²⁶⁶ Pb	82	184	266	0.31	2.24	1.22×10^{-2}	5.13×10^{-2}	0	1.73×10^1	9.37×10^{-1}	3.07×10^{-3}

TABLE V. Same as Tables I–IV, but for $B_\star = 10^5$.

AME2020 + HFB27 ($B_\star = 10^5$)											
Nuclides	Z	N	A	y_e	N/Z	n_{\max} [fm^{-3}]	P_{\max} [MeV/fm^3]	ν_{\max}	R [fm]	$\hbar\omega$ [MeV]	S [MeV/fm^3]
^{90}Zr	40	50	90	0.44	1.25	2.06×10^{-3}	1.66×10^{-3}	0	2.18×10^1	5.55×10^{-1}	2.88×10^{-4}
^{88}Sr	38	50	88	0.43	1.32	2.40×10^{-3}	2.23×10^{-3}	0	2.06×10^1	5.82×10^{-1}	3.28×10^{-4}
^{118}Sn	50	68	118	0.42	1.36	2.68×10^{-3}	2.57×10^{-3}	0	2.19×10^1	6.04×10^{-1}	4.45×10^{-4}
^{140}Ce	58	82	140	0.41	1.41	3.12×10^{-3}	3.32×10^{-3}	0	2.20×10^1	6.37×10^{-1}	5.85×10^{-4}
^{138}Ba	56	82	138	0.41	1.46	4.10×10^{-3}	5.98×10^{-3}	0	2.00×10^1	7.15×10^{-1}	8.01×10^{-4}
^{136}Xe	54	82	136	0.40	1.52	5.05×10^{-3}	9.08×10^{-3}	0	1.86×10^1	7.76×10^{-1}	1.00×10^{-3}
^{134}Te	52	82	134	0.39	1.58	5.98×10^{-3}	1.26×10^{-2}	0	1.75×10^1	8.26×10^{-1}	1.19×10^{-3}
^{132}Sn	50	82	132	0.38	1.64	7.43×10^{-3}	1.92×10^{-2}	0	1.62×10^1	8.98×10^{-1}	1.49×10^{-3}
^{202}Os	76	126	202	0.38	1.66	8.91×10^{-3}	2.63×10^{-2}	0	1.75×10^1	9.77×10^{-1}	2.50×10^{-3}
^{200}W	74	126	200	0.37	1.70	9.47×10^{-3}	2.91×10^{-2}	0	1.71×10^1	9.91×10^{-1}	2.60×10^{-3}
^{198}Hf	72	126	198	0.36	1.75	1.03×10^{-2}	3.38×10^{-2}	0	1.66×10^1	1.02×10^0	2.80×10^{-3}
^{196}Yb	70	126	196	0.36	1.80	1.07×10^{-2}	3.51×10^{-2}	0	1.64×10^1	1.02×10^0	2.81×10^{-3}
^{260}Th	90	170	260	0.35	1.89	1.13×10^{-2}	3.58×10^{-2}	0	1.76×10^1	1.01×10^0	3.44×10^{-3}
^{268}U	92	176	268	0.34	1.91	1.16×10^{-2}	3.73×10^{-2}	0	1.76×10^1	1.02×10^0	3.58×10^{-3}
^{270}U	92	178	270	0.34	1.93	1.23×10^{-2}	4.16×10^{-2}	0	1.73×10^1	1.04×10^0	3.83×10^{-3}
^{268}Th	90	178	268	0.34	1.98	1.28×10^{-2}	4.38×10^{-2}	0	1.71×10^1	1.04×10^0	3.89×10^{-3}
^{276}U	92	184	276	0.33	2.00	1.33×10^{-2}	4.69×10^{-2}	0	1.70×10^1	1.06×10^0	4.12×10^{-3}
^{274}Th	90	184	274	0.33	2.04	1.41×10^{-2}	5.13×10^{-2}	0	1.67×10^1	1.07×10^0	4.29×10^{-3}
^{272}Ra	88	184	272	0.32	2.09	1.45×10^{-2}	5.34×10^{-2}	0	1.65×10^1	1.07×10^0	4.32×10^{-3}
^{331}Hs	108	223	331	0.33	2.06	1.50×10^{-2}	5.61×10^{-2}	0	1.74×10^1	1.10×10^0	5.21×10^{-3}
^{329}Sg	106	223	329	0.32	2.10	1.54×10^{-2}	5.84×10^{-2}	0	1.72×10^1	1.10×10^0	5.26×10^{-3}
^{337}Hs	108	229	337	0.32	2.12	1.59×10^{-2}	6.14×10^{-2}	0	1.72×10^1	1.11×10^0	5.50×10^{-3}
^{333}Sg	106	227	333	0.32	2.14	1.63×10^{-2}	6.45×10^{-2}	0	1.69×10^1	1.12×10^0	5.59×10^{-3}
^{335}Sg	106	229	335	0.32	2.16	1.65×10^{-2}	6.51×10^{-2}	0	1.69×10^1	1.12×10^0	5.63×10^{-3}
^{343}Hs	108	235	343	0.31	2.18	1.69×10^{-2}	6.71×10^{-2}	0	1.69×10^1	1.12×10^0	5.82×10^{-3}
^{387}Ubn	120	267	387	0.31	2.23	1.75×10^{-2}	6.98×10^{-2}	0	1.74×10^1	1.13×10^0	6.46×10^{-3}
^{391}Ubn	120	271	391	0.31	2.26	1.79×10^{-2}	7.12×10^{-2}	0	1.73×10^1	1.13×10^0	6.54×10^{-3}
^{405}Ubb	124	281	405	0.31	2.27	1.82×10^{-2}	7.34×10^{-2}	0	1.74×10^1	1.14×10^0	6.83×10^{-3}
^{407}Ubb	124	283	407	0.30	2.28	1.84×10^{-2}	7.41×10^{-2}	0	1.74×10^1	1.14×10^0	6.87×10^{-3}
^{403}Ubb	122	281	403	0.30	2.30	1.88×10^{-2}	7.64×10^{-2}	0	1.72×10^1	1.14×10^0	6.91×10^{-3}
^{409}Ubb	122	287	409	0.30	2.35	1.92×10^{-2}	7.79×10^{-2}	0	1.72×10^1	1.14×10^0	7.00×10^{-3}

TABLE VI. Same as Table I (*i.e.* $B = 0$), but calculated with the HFB-32 mass model [32].

AME2020+HFB32 ($B = 0$)										
Nuclides	Z	N	A	y_e	N/Z	n_{\max} [fm $^{-3}$]	P_{\max} [MeV/fm 3]	R [fm]	$\hbar\omega_p$ [MeV]	S [MeV/fm 3]
^{56}Fe	26	30	56	0.46	1.15	4.94×10^{-9}	3.37×10^{-10}	1.39×10^3	8.98×10^{-4}	7.35×10^{-12}
^{62}Ni	28	34	62	0.45	1.21	1.58×10^{-7}	4.16×10^{-8}	4.54×10^2	4.94×10^{-3}	7.55×10^{-10}
^{58}Fe	26	32	58	0.45	1.23	1.65×10^{-7}	4.37×10^{-8}	4.38×10^2	5.01×10^{-3}	7.53×10^{-10}
^{64}Ni	28	36	64	0.44	1.29	7.96×10^{-7}	3.53×10^{-7}	2.68×10^2	1.07×10^{-2}	6.25×10^{-9}
^{66}Ni	28	38	66	0.42	1.36	9.24×10^{-7}	4.14×10^{-7}	2.57×10^2	1.12×10^{-2}	7.33×10^{-9}
^{86}Kr	36	50	86	0.42	1.39	1.85×10^{-6}	1.02×10^{-6}	2.23×10^2	1.57×10^{-2}	2.15×10^{-8}
^{84}Se	34	50	84	0.40	1.47	6.77×10^{-6}	5.56×10^{-6}	1.43×10^2	2.90×10^{-2}	1.11×10^{-7}
^{82}Ge	32	50	82	0.39	1.56	1.67×10^{-5}	1.76×10^{-5}	1.05×10^2	4.38×10^{-2}	3.39×10^{-7}
^{80}Zn	30	50	80	0.38	1.67	3.93×10^{-5}	5.27×10^{-5}	7.86×10^1	6.47×10^{-2}	9.66×10^{-7}
^{78}Ni	28	50	78	0.36	1.79	5.24×10^{-5}	7.31×10^{-5}	7.08×10^1	7.15×10^{-2}	1.28×10^{-6}
^{80}Ni	28	52	80	0.35	1.86	7.63×10^{-5}	1.17×10^{-4}	6.30×10^1	8.41×10^{-2}	2.04×10^{-6}
^{124}Mo	42	82	124	0.34	1.95	9.89×10^{-5}	1.56×10^{-4}	6.69×10^1	9.27×10^{-2}	3.62×10^{-6}
^{122}Zr	40	82	122	0.33	2.05	1.42×10^{-4}	2.41×10^{-4}	5.90×10^1	1.07×10^{-1}	5.41×10^{-6}
^{121}Y	39	82	121	0.32	2.10	1.65×10^{-4}	2.89×10^{-4}	5.60×10^1	1.14×10^{-1}	6.36×10^{-6}
^{120}Sr	38	82	120	0.32	2.16	1.80×10^{-4}	3.19×10^{-4}	5.41×10^1	1.17×10^{-1}	6.90×10^{-6}
^{122}Sr	38	84	122	0.31	2.21	2.26×10^{-4}	4.21×10^{-4}	5.05×10^1	1.29×10^{-1}	9.12×10^{-6}
^{124}Sr	38	86	124	0.31	2.26	2.59×10^{-4}	4.94×10^{-4}	4.85×10^1	1.36×10^{-1}	1.07×10^{-5}

TABLE VII. Same as Table VI, but for $B_* = 10^3$.

AME2020+HFB32 ($B_* = 10^3$)											
Nuclides	Z	N	A	y_e	N/Z	n_{\max} [fm $^{-3}$]	P_{\max} [MeV/fm 3]	ν_{\max}	R [fm]	$\hbar\omega$ [MeV]	S [MeV/fm 3]
^{56}Fe	26	30	56	0.46	1.15	2.62×10^{-6}	1.97×10^{-7}	0	1.72×10^2	2.07×10^{-2}	3.16×10^{-8}
^{62}Ni	28	34	62	0.45	1.21	1.10×10^{-5}	6.18×10^{-6}	0	1.10×10^2	4.12×10^{-2}	2.16×10^{-7}
^{64}Ni	28	36	64	0.44	1.29	1.42×10^{-5}	1.01×10^{-5}	0	1.02×10^2	4.54×10^{-2}	2.93×10^{-7}
^{88}Sr	38	50	88	0.43	1.32	1.55×10^{-5}	1.16×10^{-5}	0	1.11×10^2	4.68×10^{-2}	3.96×10^{-7}
^{86}Kr	36	50	86	0.42	1.39	2.60×10^{-5}	3.19×10^{-5}	0	9.25×10^1	5.87×10^{-2}	7.28×10^{-7}
^{84}Se	34	50	84	0.40	1.47	3.88×10^{-5}	6.79×10^{-5}	0	8.03×10^1	6.93×10^{-2}	1.14×10^{-6}
^{82}Ge	32	50	82	0.39	1.56	5.20×10^{-5}	1.15×10^{-4}	0	7.22×10^1	7.75×10^{-2}	1.55×10^{-6}
^{80}Zn	30	50	80	0.38	1.67	6.98×10^{-5}	1.93×10^{-4}	0	6.49×10^1	8.62×10^{-2}	2.08×10^{-6}
^{78}Ni	28	50	78	0.36	1.79	7.85×10^{-5}	2.24×10^{-4}	0	6.19×10^1	8.75×10^{-2}	2.19×10^{-6}
^{80}Ni	28	52	80	0.35	1.86	8.88×10^{-5}	2.74×10^{-4}	0	5.99×10^1	9.07×10^{-2}	2.50×10^{-6}
^{124}Mo	42	82	124	0.34	1.95	9.96×10^{-5}	3.21×10^{-4}	0	6.67×10^1	9.30×10^{-2}	3.65×10^{-6}
^{122}Zr	40	82	122	0.33	2.05	1.15×10^{-4}	3.99×10^{-4}	0	6.33×10^1	9.66×10^{-2}	4.08×10^{-6}
^{121}Y	39	82	121	0.32	2.10	1.21×10^{-4}	4.32×10^{-4}	0	6.20×10^1	9.76×10^{-2}	4.23×10^{-6}
^{120}Sr	38	82	120	0.32	2.16	1.91×10^{-4}	4.68×10^{-4}	0, 1	5.31×10^1	1.20×10^{-1}	7.43×10^{-6}
^{122}Sr	38	84	122	0.31	2.21	2.60×10^{-4}	5.83×10^{-4}	1	4.82×10^1	1.38×10^{-1}	1.10×10^{-5}
^{124}Sr	38	86	124	0.31	2.26	2.94×10^{-4}	6.63×10^{-4}	1	4.65×10^1	1.44×10^{-1}	1.26×10^{-5}

TABLE VIII. Same as Tables VI and VII, but for $B_\star = 3 \times 10^4$.

AME2020 + HFB32 ($B_\star = 3 \times 10^4$)											
Nuclides	Z	N	A	y_e	N/Z	$n_{\max} [\text{fm}^{-3}]$	$P_{\max} [\text{MeV}/\text{fm}^3]$	ν_{\max}	$R [\text{fm}]$	$\hbar\omega [\text{MeV}]$	$S [\text{MeV}/\text{fm}^3]$
^{60}Ni	28	32	60	0.47	1.14	1.37×10^{-4}	1.56×10^{-5}	0	4.71×10^1	1.50×10^{-1}	6.54×10^{-6}
^{90}Zr	40	50	90	0.44	1.25	2.88×10^{-4}	9.43×10^{-5}	0	4.21×10^1	2.08×10^{-1}	2.09×10^{-5}
^{88}Sr	38	50	88	0.43	1.32	8.27×10^{-4}	1.02×10^{-3}	0	2.94×10^1	3.42×10^{-1}	7.94×10^{-5}
^{86}Kr	36	50	86	0.42	1.39	1.01×10^{-3}	1.48×10^{-3}	0	2.73×10^1	3.67×10^{-1}	9.65×10^{-5}
^{128}Sn	50	78	128	0.39	1.56	1.13×10^{-3}	1.54×10^{-3}	0	3.00×10^1	3.61×10^{-1}	1.26×10^{-4}
^{134}Te	52	82	134	0.39	1.58	1.31×10^{-3}	2.10×10^{-3}	0	2.90×10^1	3.87×10^{-1}	1.57×10^{-4}
^{132}Sn	50	82	132	0.38	1.64	2.52×10^{-3}	7.90×10^{-3}	0	2.32×10^1	5.23×10^{-1}	3.53×10^{-4}
^{128}Pd	46	82	128	0.36	1.78	3.09×10^{-3}	1.09×10^{-2}	0	2.15×10^1	5.49×10^{-1}	4.08×10^{-4}
^{126}Ru	44	82	126	0.35	1.86	3.23×10^{-3}	1.13×10^{-2}	0	2.10×10^1	5.46×10^{-1}	4.06×10^{-4}
^{188}Sm	62	126	188	0.33	2.03	3.61×10^{-3}	1.24×10^{-2}	0	2.31×10^1	5.45×10^{-1}	5.49×10^{-4}
^{186}Nd	60	126	186	0.32	2.10	3.89×10^{-3}	1.38×10^{-2}	0	2.25×10^1	5.53×10^{-1}	5.75×10^{-4}
^{184}Ce	58	126	184	0.32	2.17	4.46×10^{-3}	1.75×10^{-2}	0	2.14×10^1	5.79×10^{-1}	6.55×10^{-4}
^{182}Ba	56	126	182	0.31	2.25	4.73×10^{-3}	1.88×10^{-2}	0	2.09×10^1	5.82×10^{-1}	6.68×10^{-4}
^{180}Xe	54	126	180	0.30	2.33	4.99×10^{-3}	1.99×10^{-2}	0	2.05×10^1	5.82×10^{-1}	6.77×10^{-4}

TABLE IX. Same as Tables VI–VIII, but for $B_\star = 7 \times 10^4$.

AME2020 + HFB32 ($B_\star = 7 \times 10^4$)											
Nuclides	Z	N	A	y_e	N/Z	$n_{\max} [\text{fm}^{-3}]$	$P_{\max} [\text{MeV}/\text{fm}^3]$	ν_{\max}	$R [\text{fm}]$	$\hbar\omega [\text{MeV}]$	$S [\text{MeV}/\text{fm}^3]$
^{90}Zr	40	50	90	0.44	1.25	1.17×10^{-3}	7.47×10^{-4}	0	2.64×10^1	4.18×10^{-1}	1.36×10^{-4}
^{88}Sr	38	50	88	0.43	1.32	1.95×10^{-3}	2.28×10^{-3}	0	2.21×10^1	5.25×10^{-1}	2.49×10^{-4}
^{138}Ba	56	82	138	0.41	1.46	2.47×10^{-3}	3.10×10^{-3}	0	2.37×10^1	5.55×10^{-1}	4.07×10^{-4}
^{136}Xe	54	82	136	0.40	1.52	3.13×10^{-3}	5.05×10^{-3}	0	2.18×10^1	6.12×10^{-1}	5.30×10^{-4}
^{134}Te	52	82	134	0.39	1.58	3.79×10^{-3}	7.30×10^{-3}	0	2.04×10^1	6.57×10^{-1}	6.45×10^{-4}
^{132}Sn	50	82	132	0.38	1.64	6.27×10^{-3}	2.03×10^{-2}	0	1.71×10^1	8.25×10^{-1}	1.19×10^{-3}
^{196}Yb	70	126	196	0.36	1.80	6.99×10^{-3}	2.18×10^{-2}	0	1.88×10^1	8.21×10^{-1}	1.59×10^{-3}
^{194}Er	68	126	194	0.35	1.85	7.45×10^{-3}	2.41×10^{-2}	0	1.84×10^1	8.32×10^{-1}	1.66×10^{-3}
^{192}Dy	66	126	192	0.34	1.91	7.99×10^{-3}	2.69×10^{-2}	0	1.79×10^1	8.45×10^{-1}	1.74×10^{-3}
^{190}Gd	64	126	190	0.34	1.97	8.45×10^{-3}	2.91×10^{-2}	0	1.75×10^1	8.52×10^{-1}	1.79×10^{-3}
^{276}U	92	184	276	0.33	2.00	8.75×10^{-3}	2.94×10^{-2}	0	1.96×10^1	8.58×10^{-1}	2.35×10^{-3}
^{274}Th	90	184	274	0.33	2.04	9.21×10^{-3}	3.18×10^{-2}	0	1.92×10^1	8.67×10^{-1}	2.44×10^{-3}
^{272}Ra	88	184	272	0.32	2.09	9.65×10^{-3}	3.41×10^{-2}	0	1.89×10^1	8.74×10^{-1}	2.50×10^{-3}
^{270}Rn	86	184	270	0.32	2.14	1.01×10^{-2}	3.62×10^{-2}	0	1.86×10^1	8.79×10^{-1}	2.55×10^{-3}
^{268}Po	84	184	268	0.31	2.19	1.05×10^{-2}	3.84×10^{-2}	0	1.82×10^1	8.83×10^{-1}	2.60×10^{-3}
^{266}Pb	82	184	266	0.31	2.24	1.23×10^{-2}	5.18×10^{-2}	0	1.73×10^1	9.40×10^{-1}	3.09×10^{-3}

TABLE X. Same as Tables VI–IX, but for $B_* = 10^5$.

AME2020 + HFB32 ($B_* = 10^5$)												
Nuclides	Z	N	A	y_e	N/Z	n_{\max} [fm^{-3}]	P_{\max} [MeV/fm^3]	ν_{\max}	R [fm]	$\hbar\omega$ [MeV]	S [MeV/fm^3]	
⁹⁰ Zr	40	50	90	0.44	1.25	2.06×10^{-3}	1.66×10^{-3}	0	2.18×10^1	5.55×10^{-1}	2.88×10^{-4}	
⁸⁸ Sr	38	50	88	0.43	1.32	2.40×10^{-3}	2.23×10^{-3}	0	2.06×10^1	5.82×10^{-1}	3.28×10^{-4}	
¹¹⁸ Sn	50	68	118	0.42	1.36	2.68×10^{-3}	2.57×10^{-3}	0	2.19×10^1	6.04×10^{-1}	4.45×10^{-4}	
¹⁴⁰ Ce	58	82	140	0.41	1.41	3.12×10^{-3}	3.32×10^{-3}	0	2.20×10^1	6.37×10^{-1}	5.85×10^{-4}	
¹³⁸ Ba	56	82	138	0.41	1.46	4.10×10^{-3}	5.98×10^{-3}	0	2.00×10^1	7.15×10^{-1}	8.01×10^{-4}	
¹³⁶ Xe	54	82	136	0.40	1.52	5.05×10^{-3}	9.08×10^{-3}	0	1.86×10^1	7.76×10^{-1}	1.00×10^{-3}	
¹³⁴ Te	52	82	134	0.39	1.58	5.98×10^{-3}	1.26×10^{-2}	0	1.75×10^1	8.26×10^{-1}	1.19×10^{-3}	
¹³² Sn	50	82	132	0.38	1.64	7.78×10^{-3}	2.12×10^{-2}	0	1.59×10^1	9.19×10^{-1}	1.59×10^{-3}	
²⁰² Os	76	126	202	0.38	1.66	8.75×10^{-3}	2.53×10^{-2}	0	1.77×10^1	9.68×10^{-1}	2.44×10^{-3}	
²⁰⁰ W	74	126	200	0.37	1.70	9.43×10^{-3}	2.88×10^{-2}	0	1.72×10^1	9.88×10^{-1}	2.58×10^{-3}	
¹⁹⁸ Hf	72	126	198	0.36	1.75	1.00×10^{-2}	3.18×10^{-2}	0	1.68×10^1	1.00×10^0	2.69×10^{-3}	
²⁶⁶ U	92	174	266	0.35	1.89	1.09×10^{-2}	3.28×10^{-2}	0	1.80×10^1	9.92×10^{-1}	3.31×10^{-3}	
²⁶⁸ U	92	176	268	0.34	1.91	1.11×10^{-2}	3.34×10^{-2}	0	1.79×10^1	9.93×10^{-1}	3.35×10^{-3}	
²⁷⁰ U	92	178	270	0.34	1.93	1.16×10^{-2}	3.62×10^{-2}	0	1.77×10^1	1.01×10^0	3.51×10^{-3}	
²⁷² U	92	180	272	0.34	1.96	1.17×10^{-2}	3.69×10^{-2}	0	1.77×10^1	1.01×10^0	3.56×10^{-3}	
²⁷⁴ U	92	182	274	0.34	1.98	1.22×10^{-2}	3.96×10^{-2}	0	1.75×10^1	1.02×10^0	3.71×10^{-3}	
²⁷⁶ U	92	184	276	0.33	2.00	1.37×10^{-2}	4.98×10^{-2}	0	1.69×10^1	1.07×10^0	4.28×10^{-3}	
²⁷⁴ Th	90	184	274	0.33	2.04	1.43×10^{-2}	5.29×10^{-2}	0	1.66×10^1	1.08×10^0	4.37×10^{-3}	
²⁷² Ra	88	184	272	0.32	2.09	1.49×10^{-2}	5.61×10^{-2}	0	1.63×10^1	1.08×10^0	4.46×10^{-3}	
²⁷⁰ Rn	86	184	270	0.32	2.14	1.55×10^{-2}	5.96×10^{-2}	0	1.61×10^1	1.09×10^0	4.55×10^{-3}	
²⁶⁸ Po	84	184	268	0.31	2.19	1.61×10^{-2}	6.26×10^{-2}	0	1.58×10^1	1.09×10^0	4.61×10^{-3}	
²⁶⁶ Pb	82	184	266	0.31	2.24	1.72×10^{-2}	6.91×10^{-2}	0	1.55×10^1	1.11×10^0	4.82×10^{-3}	
³⁷⁵ Mc	115	260	375	0.31	2.26	1.79×10^{-2}	7.12×10^{-2}	0	1.71×10^1	1.13×10^0	6.33×10^{-3}	
³⁷⁶ Mc	115	261	376	0.31	2.27	1.80×10^{-2}	7.20×10^{-2}	0	1.71×10^1	1.13×10^0	6.37×10^{-3}	
³⁷⁷ Mc	115	262	377	0.31	2.28	1.82×10^{-2}	7.34×10^{-2}	0	1.70×10^1	1.13×10^0	6.45×10^{-3}	
³⁷⁹ Mc	115	264	379	0.30	2.30	1.84×10^{-2}	7.41×10^{-2}	0	1.70×10^1	1.13×10^0	6.49×10^{-3}	
³⁹⁶ Uue	119	277	396	0.30	2.33	1.88×10^{-2}	7.56×10^{-2}	0	1.71×10^1	1.13×10^0	6.74×10^{-3}	
⁴⁰⁰ Uue	119	281	400	0.30	2.36	1.92×10^{-2}	7.79×10^{-2}	0	1.71×10^1	1.13×10^0	6.87×10^{-3}	
⁴⁰² Uue	119	283	402	0.30	2.38	1.94×10^{-2}	7.87×10^{-2}	0	1.70×10^1	1.13×10^0	6.91×10^{-3}	

TABLE XI. Same as Table I (*i.e.* $B = 0$), but calculated with the BML mass model [33].

AME2020 + BML ($B = 0$)										
Nuclides	Z	N	A	y_e	N/Z	n_{\max} [fm^{-3}]	P_{\max} [MeV/fm^3]	R [fm]	$\hbar\omega$ [MeV]	S [MeV/fm^3]
^{56}Fe	26	30	56	0.46	1.15	4.94×10^{-9}	3.37×10^{-10}	1.39×10^3	8.98×10^{-4}	7.35×10^{-12}
^{62}Ni	28	34	62	0.45	1.21	1.58×10^{-7}	4.16×10^{-8}	4.54×10^2	4.94×10^{-3}	7.55×10^{-10}
^{58}Fe	26	32	58	0.45	1.23	1.65×10^{-7}	4.37×10^{-8}	4.38×10^2	5.01×10^{-3}	7.53×10^{-10}
^{64}Ni	28	36	64	0.44	1.29	7.96×10^{-7}	3.53×10^{-7}	2.68×10^2	1.07×10^{-2}	6.25×10^{-9}
^{66}Ni	28	38	66	0.42	1.36	9.24×10^{-7}	4.14×10^{-7}	2.57×10^2	1.12×10^{-2}	7.33×10^{-9}
^{86}Kr	36	50	86	0.42	1.39	1.85×10^{-6}	1.02×10^{-6}	2.23×10^2	1.57×10^{-2}	2.15×10^{-8}
^{84}Se	34	50	84	0.40	1.47	6.77×10^{-6}	5.56×10^{-6}	1.43×10^2	2.90×10^{-2}	1.11×10^{-7}
^{82}Ge	32	50	82	0.39	1.56	1.67×10^{-5}	1.76×10^{-5}	1.05×10^2	4.38×10^{-2}	3.39×10^{-7}
^{80}Zn	30	50	80	0.38	1.67	3.24×10^{-5}	4.06×10^{-5}	8.39×10^1	5.87×10^{-2}	7.46×10^{-7}
^{78}Ni	28	50	78	0.36	1.79	7.22×10^{-5}	1.12×10^{-4}	6.36×10^1	8.39×10^{-2}	1.96×10^{-6}
^{80}Ni	28	52	80	0.35	1.86	8.73×10^{-5}	1.40×10^{-4}	6.03×10^1	9.00×10^{-2}	2.44×10^{-6}
^{124}Mo	42	82	124	0.34	1.95	1.07×10^{-4}	1.72×10^{-4}	6.52×10^1	9.62×10^{-2}	4.00×10^{-6}
^{122}Zr	40	82	122	0.33	2.05	1.56×10^{-4}	2.75×10^{-4}	5.71×10^1	1.13×10^{-1}	6.16×10^{-6}
^{120}Sr	38	82	120	0.32	2.16	2.24×10^{-4}	4.25×10^{-4}	5.04×10^1	1.30×10^{-1}	9.21×10^{-6}
^{118}Kr	36	82	118	0.31	2.28	2.58×10^{-4}	4.89×10^{-4}	4.78×10^1	1.35×10^{-1}	1.02×10^{-5}

TABLE XII. Same as Table XI, but for $B_* = 10^3$.

AME2020 + BML ($B_* = 10^3$)											
Nuclides	Z	N	A	y_e	N/Z	n_{\max} [fm^{-3}]	P_{\max} [MeV/fm^3]	ν_{\max}	R [fm]	$\hbar\omega$ [MeV]	S [MeV/fm^3]
^{56}Fe	26	30	56	0.46	1.15	2.62×10^{-6}	1.97×10^{-7}	0	1.72×10^2	2.07×10^{-2}	3.16×10^{-8}
^{62}Ni	28	34	62	0.45	1.21	1.10×10^{-5}	6.18×10^{-6}	0	1.10×10^2	4.12×10^{-2}	2.16×10^{-7}
^{64}Ni	28	36	64	0.44	1.29	1.42×10^{-5}	1.01×10^{-5}	0	1.02×10^2	4.54×10^{-2}	2.93×10^{-7}
^{88}Sr	38	50	88	0.43	1.32	1.55×10^{-5}	1.16×10^{-5}	0	1.11×10^2	4.68×10^{-2}	3.96×10^{-7}
^{86}Kr	36	50	86	0.42	1.39	2.60×10^{-5}	3.19×10^{-5}	0	9.25×10^1	5.87×10^{-2}	7.28×10^{-7}
^{84}Se	34	50	84	0.40	1.47	3.88×10^{-5}	6.79×10^{-5}	0	8.03×10^1	6.93×10^{-2}	1.14×10^{-6}
^{82}Ge	32	50	82	0.39	1.56	5.20×10^{-5}	1.15×10^{-4}	0	7.22×10^1	7.75×10^{-2}	1.55×10^{-6}
^{80}Zn	30	50	80	0.38	1.67	6.55×10^{-5}	1.70×10^{-4}	0	6.63×10^1	8.35×10^{-2}	1.91×10^{-6}
^{78}Ni	28	50	78	0.36	1.79	8.70×10^{-5}	2.76×10^{-4}	0	5.98×10^1	9.21×10^{-2}	2.51×10^{-6}
^{80}Ni	28	52	80	0.35	1.86	9.33×10^{-5}	3.02×10^{-4}	0	5.89×10^1	9.30×10^{-2}	2.67×10^{-6}
^{124}Mo	42	82	124	0.34	1.95	1.02×10^{-4}	3.37×10^{-4}	0	6.62×10^1	9.41×10^{-2}	3.77×10^{-6}
^{122}Zr	40	82	122	0.33	2.05	1.18×10^{-4}	4.24×10^{-4}	0	6.27×10^1	9.80×10^{-2}	4.25×10^{-6}
^{120}Sr	38	82	120	0.32	2.16	2.58×10^{-4}	5.89×10^{-4}	0, 1	4.81×10^1	1.40×10^{-1}	1.11×10^{-5}
^{118}Kr	36	82	118	0.31	2.28	2.92×10^{-4}	6.57×10^{-4}	1	4.58×10^1	1.43×10^{-1}	1.20×10^{-5}

TABLE XIII. Same as Tables XI and XII, but for $B_* = 3 \times 10^4$.

AME2020 + BML ($B_* = 3 \times 10^4$)											
Nuclides	Z	N	A	y_e	N/Z	$n_{\max} [\text{fm}^{-3}]$	$P_{\max} [\text{MeV}/\text{fm}^3]$	ν_{\max}	$R [\text{fm}]$	$\hbar\omega [\text{MeV}]$	$S [\text{MeV}/\text{fm}^3]$
⁶⁰ Ni	28	32	60	0.47	1.14	1.37×10^{-4}	1.56×10^{-5}	0	4.71×10^1	1.50×10^{-1}	6.54×10^{-6}
⁹⁰ Zr	40	50	90	0.44	1.25	2.88×10^{-4}	9.43×10^{-5}	0	4.21×10^1	2.08×10^{-1}	2.09×10^{-5}
⁸⁸ Sr	38	50	88	0.43	1.32	8.27×10^{-4}	1.02×10^{-3}	0	2.94×10^1	3.42×10^{-1}	7.94×10^{-5}
⁸⁶ Kr	36	50	86	0.42	1.39	1.01×10^{-3}	1.48×10^{-3}	0	2.73×10^1	3.67×10^{-1}	9.65×10^{-5}
¹²⁸ Sn	50	78	128	0.39	1.56	1.13×10^{-3}	1.54×10^{-3}	0	3.00×10^1	3.61×10^{-1}	1.26×10^{-4}
¹³⁴ Te	52	82	134	0.39	1.58	1.31×10^{-3}	2.10×10^{-3}	0	2.90×10^1	3.87×10^{-1}	1.57×10^{-4}
¹³² Sn	50	82	132	0.38	1.64	2.53×10^{-3}	7.98×10^{-3}	0	2.32×10^1	5.24×10^{-1}	3.55×10^{-4}
¹³⁰ Cd	48	82	130	0.37	1.71	2.75×10^{-3}	8.99×10^{-3}	0	2.24×10^1	5.32×10^{-1}	3.73×10^{-4}
¹²⁸ Pd	46	82	128	0.36	1.78	3.04×10^{-3}	1.05×10^{-2}	0	2.16×10^1	5.45×10^{-1}	4.01×10^{-4}
¹²⁶ Ru	44	82	126	0.35	1.86	3.16×10^{-3}	1.07×10^{-2}	0	2.12×10^1	5.40×10^{-1}	3.93×10^{-4}
¹⁶⁶ Ba	56	110	166	0.34	1.96	3.39×10^{-3}	1.14×10^{-2}	0	2.27×10^1	5.40×10^{-1}	4.85×10^{-4}
¹⁶⁸ Ba	56	112	168	0.33	2.00	3.58×10^{-3}	1.25×10^{-2}	0	2.24×10^1	5.49×10^{-1}	5.14×10^{-4}
¹⁷⁰ Ba	56	114	170	0.33	2.04	3.73×10^{-3}	1.33×10^{-2}	0	2.21×10^1	5.53×10^{-1}	5.34×10^{-4}
¹⁷² Ba	56	116	172	0.33	2.07	4.00×10^{-3}	1.49×10^{-2}	0	2.17×10^1	5.66×10^{-1}	5.77×10^{-4}
¹⁸² Ce	58	124	182	0.32	2.14	4.17×10^{-3}	1.55×10^{-2}	0	2.18×10^1	5.66×10^{-1}	6.07×10^{-4}
¹⁸⁴ Ce	58	126	184	0.32	2.17	4.42×10^{-3}	1.72×10^{-2}	0	2.15×10^1	5.76×10^{-1}	6.47×10^{-4}
¹⁸² Ba	56	126	182	0.31	2.25	4.77×10^{-3}	1.92×10^{-2}	0	2.09×10^1	5.84×10^{-1}	6.77×10^{-4}
¹⁸⁰ Xe	54	126	180	0.30	2.33	4.99×10^{-3}	1.99×10^{-2}	0	2.05×10^1	5.82×10^{-1}	6.77×10^{-4}

TABLE XIV. Same as Tables XI–XIII, but for $B_* = 7 \times 10^4$.

AME2020 + BML ($B_* = 7 \times 10^4$)											
Nuclides	Z	N	A	y_e	N/Z	$n_{\max} [\text{fm}^{-3}]$	$P_{\max} [\text{MeV}/\text{fm}^3]$	ν_{\max}	$R [\text{fm}]$	$\hbar\omega [\text{MeV}]$	$S [\text{MeV}/\text{fm}^3]$
⁹⁰ Zr	40	50	90	0.44	1.25	1.17×10^{-3}	7.47×10^{-4}	0	2.64×10^1	4.18×10^{-1}	1.36×10^{-4}
⁸⁸ Sr	38	50	88	0.43	1.32	1.95×10^{-3}	2.28×10^{-3}	0	2.21×10^1	5.25×10^{-1}	2.49×10^{-4}
¹³⁸ Ba	56	82	138	0.41	1.46	2.47×10^{-3}	3.10×10^{-3}	0	2.37×10^1	5.55×10^{-1}	4.07×10^{-4}
¹³⁶ Xe	54	82	136	0.40	1.52	3.13×10^{-3}	5.05×10^{-3}	0	2.18×10^1	6.12×10^{-1}	5.30×10^{-4}
¹³⁴ Te	52	82	134	0.39	1.58	3.79×10^{-3}	7.30×10^{-3}	0	2.04×10^1	6.57×10^{-1}	6.45×10^{-4}
¹³² Sn	50	82	132	0.38	1.64	6.30×10^{-3}	2.05×10^{-2}	0	1.71×10^1	8.27×10^{-1}	1.20×10^{-3}
²⁰⁸ W	74	134	208	0.36	1.81	7.07×10^{-3}	2.20×10^{-2}	0	1.91×10^1	8.23×10^{-1}	1.67×10^{-3}
²⁰⁴ Hf	72	132	204	0.35	1.83	7.18×10^{-3}	2.25×10^{-2}	0	1.89×10^1	8.23×10^{-1}	1.66×10^{-3}
²⁰⁶ Hf	72	134	206	0.35	1.86	7.85×10^{-3}	2.66×10^{-2}	0	1.84×10^1	8.52×10^{-1}	1.84×10^{-3}
²⁰⁴ Yb	70	134	204	0.34	1.91	8.30×10^{-3}	2.88×10^{-2}	0	1.80×10^1	8.60×10^{-1}	1.90×10^{-3}
²⁷⁶ U	92	184	276	0.33	2.00	8.92×10^{-3}	3.06×10^{-2}	0	1.95×10^1	8.66×10^{-1}	2.42×10^{-3}
²⁷² Th	90	182	272	0.33	2.02	9.02×10^{-3}	3.09×10^{-2}	0	1.93×10^1	8.64×10^{-1}	2.39×10^{-3}
²⁷⁴ Th	90	184	274	0.33	2.04	9.56×10^{-3}	3.44×10^{-2}	0	1.90×10^1	8.83×10^{-1}	2.56×10^{-3}
²⁷² Ra	88	184	272	0.32	2.09	1.02×10^{-2}	3.81×10^{-2}	0	1.85×10^1	8.96×10^{-1}	2.68×10^{-3}
²⁷⁰ Rn	86	184	270	0.32	2.14	1.07×10^{-2}	4.12×10^{-2}	0	1.82×10^1	9.06×10^{-1}	2.77×10^{-3}
²⁶⁸ Po	84	184	268	0.31	2.19	1.11×10^{-2}	4.33×10^{-2}	0	1.79×10^1	9.09×10^{-1}	2.81×10^{-3}
²⁶⁶ Pb	82	184	266	0.31	2.24	1.22×10^{-2}	5.13×10^{-2}	0	1.73×10^1	9.37×10^{-1}	3.07×10^{-3}

TABLE XV. Same as Tables XI–XIV, but for $B_* = 10^5$.

AME2020+BML ($B_* = 10^5$)											
Nuclides	Z	N	A	y_e	N/Z	n_{\max} [fm $^{-3}$]	P_{\max} [MeV/fm 3]	ν_{\max}	R [fm]	$\hbar\omega$ [MeV]	S [MeV/fm 3]
^{90}Zr	40	50	90	0.44	1.25	2.06×10^{-3}	1.66×10^{-3}	0	2.18×10^1	5.55×10^{-1}	2.88×10^{-4}
^{88}Sr	38	50	88	0.43	1.32	2.40×10^{-3}	2.23×10^{-3}	0	2.06×10^1	5.82×10^{-1}	3.28×10^{-4}
^{118}Sn	50	68	118	0.42	1.36	2.68×10^{-3}	2.57×10^{-3}	0	2.19×10^1	6.04×10^{-1}	4.45×10^{-4}
^{140}Ce	58	82	140	0.41	1.41	3.12×10^{-3}	3.32×10^{-3}	0	2.20×10^1	6.37×10^{-1}	5.85×10^{-4}
^{138}Ba	56	82	138	0.41	1.46	4.10×10^{-3}	5.98×10^{-3}	0	2.00×10^1	7.15×10^{-1}	8.01×10^{-4}
^{136}Xe	54	82	136	0.40	1.52	5.05×10^{-3}	9.08×10^{-3}	0	1.86×10^1	7.76×10^{-1}	1.00×10^{-3}
^{134}Te	52	82	134	0.39	1.58	5.98×10^{-3}	1.26×10^{-2}	0	1.75×10^1	8.26×10^{-1}	1.19×10^{-3}
^{132}Sn	50	82	132	0.38	1.64	7.56×10^{-3}	1.99×10^{-2}	0	1.61×10^1	9.06×10^{-1}	1.53×10^{-3}
^{204}Pt	78	126	204	0.38	1.62	7.95×10^{-3}	2.12×10^{-2}	0	1.83×10^1	9.38×10^{-1}	2.23×10^{-3}
^{202}Os	76	126	202	0.38	1.66	8.91×10^{-3}	2.63×10^{-2}	0	1.75×10^1	9.77×10^{-1}	2.50×10^{-3}
^{200}W	74	126	200	0.37	1.70	9.47×10^{-3}	2.91×10^{-2}	0	1.71×10^1	9.91×10^{-1}	2.60×10^{-3}
^{208}W	74	134	208	0.36	1.81	1.05×10^{-2}	3.34×10^{-2}	0	1.68×10^1	1.00×10^0	2.84×10^{-3}
^{272}Pu	94	178	272	0.35	1.89	1.11×10^{-2}	3.41×10^{-2}	0	1.80×10^1	1.00×10^0	3.44×10^{-3}
^{268}U	92	176	268	0.34	1.91	1.14×10^{-2}	3.55×10^{-2}	0	1.78×10^1	1.01×10^0	3.47×10^{-3}
^{270}U	92	178	270	0.34	1.93	1.17×10^{-2}	3.73×10^{-2}	0	1.76×10^1	1.01×10^0	3.58×10^{-3}
^{272}U	92	180	272	0.34	1.96	1.22×10^{-2}	4.00×10^{-2}	0	1.75×10^1	1.03×10^0	3.74×10^{-3}
^{274}U	92	182	274	0.34	1.98	1.27×10^{-2}	4.33×10^{-2}	0	1.72×10^1	1.04×10^0	3.93×10^{-3}
^{276}U	92	184	276	0.33	2.00	1.40×10^{-2}	5.18×10^{-2}	0	1.68×10^1	1.08×10^0	4.39×10^{-3}
^{274}Th	90	184	274	0.33	2.04	1.45×10^{-2}	5.45×10^{-2}	0	1.65×10^1	1.09×10^0	4.45×10^{-3}
^{338}Ds	110	228	338	0.33	2.07	1.52×10^{-2}	5.78×10^{-2}	0	1.74×10^1	1.10×10^0	5.38×10^{-3}
^{339}Mt	109	230	339	0.32	2.11	1.56×10^{-2}	5.96×10^{-2}	0	1.73×10^1	1.10×10^0	5.44×10^{-3}
^{338}Hs	108	230	338	0.32	2.13	1.63×10^{-2}	6.45×10^{-2}	0	1.70×10^1	1.12×10^0	5.67×10^{-3}
^{339}Bh	107	232	339	0.32	2.17	1.68×10^{-2}	6.71×10^{-2}	0	1.69×10^1	1.12×10^0	5.78×10^{-3}
^{338}Sg	106	232	338	0.31	2.19	1.74×10^{-2}	7.20×10^{-2}	0	1.67×10^1	1.14×10^0	5.99×10^{-3}
^{339}Db	105	234	339	0.31	2.23	1.81×10^{-2}	7.56×10^{-2}	0	1.65×10^1	1.14×10^0	6.13×10^{-3}
^{338}Rf	104	234	338	0.31	2.25	1.84×10^{-2}	7.79×10^{-2}	0	1.64×10^1	1.15×10^0	6.20×10^{-3}

TABLE XVI. Same as Table I (*i.e.* $B = 0$), but calculated with the KTUY mass model [34].

AME2020+KTUY ($B = 0$)										
Nuclides	Z	N	A	y_e	N/Z	n_{\max} [fm^{-3}]	P_{\max} [MeV/fm^3]	R [fm]	$\hbar\omega$ [MeV]	S [MeV/fm^3]
⁵⁶ Fe	26	30	56	0.46	1.15	4.94×10^{-9}	3.37×10^{-10}	1.39×10^3	8.98×10^{-4}	7.35×10^{-12}
⁶² Ni	28	34	62	0.45	1.21	1.58×10^{-7}	4.16×10^{-8}	4.54×10^2	4.94×10^{-3}	7.55×10^{-10}
⁵⁸ Fe	26	32	58	0.45	1.23	1.65×10^{-7}	4.37×10^{-8}	4.38×10^2	5.01×10^{-3}	7.53×10^{-10}
⁶⁴ Ni	28	36	64	0.44	1.29	7.96×10^{-7}	3.53×10^{-7}	2.68×10^2	1.07×10^{-2}	6.25×10^{-9}
⁶⁶ Ni	28	38	66	0.42	1.36	9.24×10^{-7}	4.14×10^{-7}	2.57×10^2	1.12×10^{-2}	7.33×10^{-9}
⁸⁶ Kr	36	50	86	0.42	1.39	1.85×10^{-6}	1.02×10^{-6}	2.23×10^2	1.57×10^{-2}	2.15×10^{-8}
⁸⁴ Se	34	50	84	0.40	1.47	6.77×10^{-6}	5.56×10^{-6}	1.43×10^2	2.90×10^{-2}	1.11×10^{-7}
⁸² Ge	32	50	82	0.39	1.56	1.67×10^{-5}	1.76×10^{-5}	1.05×10^2	4.38×10^{-2}	3.39×10^{-7}
⁸⁰ Zn	30	50	80	0.38	1.67	2.15×10^{-5}	2.35×10^{-5}	9.62×10^1	4.78×10^{-2}	4.32×10^{-7}
⁷⁸ Ni	28	50	78	0.36	1.79	8.14×10^{-5}	1.31×10^{-4}	6.12×10^1	8.91×10^{-2}	2.30×10^{-6}
¹²⁴ Mo	42	82	124	0.34	1.95	1.01×10^{-4}	1.60×10^{-4}	6.64×10^1	9.37×10^{-2}	3.73×10^{-6}
¹²² Zr	40	82	122	0.33	2.05	1.47×10^{-4}	2.54×10^{-4}	5.83×10^1	1.09×10^{-1}	5.69×10^{-6}
¹²⁰ Sr	38	82	120	0.32	2.16	2.29×10^{-4}	4.38×10^{-4}	5.00×10^1	1.32×10^{-1}	9.48×10^{-6}
¹²² Sr	38	84	122	0.31	2.21	2.35×10^{-4}	4.43×10^{-4}	4.99×10^1	1.31×10^{-1}	9.58×10^{-6}
¹¹⁹ Kr	36	83	119	0.30	2.31	2.47×10^{-4}	4.56×10^{-4}	4.86×10^1	1.31×10^{-1}	9.50×10^{-6}
¹²⁰ Kr	36	84	120	0.30	2.33	2.64×10^{-4}	4.94×10^{-4}	4.77×10^1	1.34×10^{-1}	1.03×10^{-5}

TABLE XVII. Same as Table XVI, but for $B_* = 10^3$.

AME2020+KTUY ($B_* = 10^3$)											
Nuclides	Z	N	A	y_e	N/Z	n_{\max} [fm^{-3}]	P_{\max} [MeV/fm^3]	ν_{\max}	R [fm]	$\hbar\omega$ [MeV]	S [MeV/fm^3]
⁵⁶ Fe	26	30	56	0.46	1.15	2.62×10^{-6}	1.97×10^{-7}	0	1.72×10^2	2.07×10^{-2}	3.16×10^{-8}
⁶² Ni	28	34	62	0.45	1.21	1.10×10^{-5}	6.18×10^{-6}	0	1.10×10^2	4.12×10^{-2}	2.16×10^{-7}
⁶⁴ Ni	28	36	64	0.44	1.29	1.42×10^{-5}	1.01×10^{-5}	0	1.02×10^2	4.54×10^{-2}	2.93×10^{-7}
⁸⁸ Sr	38	50	88	0.43	1.32	1.55×10^{-5}	1.16×10^{-5}	0	1.11×10^2	4.68×10^{-2}	3.96×10^{-7}
⁸⁶ Kr	36	50	86	0.42	1.39	2.60×10^{-5}	3.19×10^{-5}	0	9.25×10^1	5.87×10^{-2}	7.28×10^{-7}
⁸⁴ Se	34	50	84	0.40	1.47	3.88×10^{-5}	6.79×10^{-5}	0	8.03×10^1	6.93×10^{-2}	1.14×10^{-6}
⁸² Ge	32	50	82	0.39	1.56	5.20×10^{-5}	1.15×10^{-4}	0	7.22×10^1	7.75×10^{-2}	1.55×10^{-6}
⁸⁰ Zn	30	50	80	0.38	1.67	5.79×10^{-5}	1.32×10^{-4}	0	6.91×10^1	7.85×10^{-2}	1.62×10^{-6}
⁷⁸ Ni	28	50	78	0.36	1.79	8.96×10^{-5}	2.93×10^{-4}	0	5.92×10^1	9.35×10^{-2}	2.62×10^{-6}
¹²⁴ Mo	42	82	124	0.34	1.95	1.01×10^{-4}	3.27×10^{-4}	0	6.65×10^1	9.35×10^{-2}	3.70×10^{-6}
¹²² Zr	40	82	122	0.33	2.05	1.16×10^{-4}	4.07×10^{-4}	0	6.31×10^1	9.70×10^{-2}	4.14×10^{-6}
¹²⁰ Sr	38	82	120	0.32	2.16	2.62×10^{-4}	6.00×10^{-4}	0, 1	4.78×10^1	1.41×10^{-1}	1.14×10^{-5}
¹²² Sr	38	84	122	0.31	2.21	2.71×10^{-4}	6.12×10^{-4}	1	4.75×10^1	1.41×10^{-1}	1.16×10^{-5}
¹¹⁹ Kr	36	83	119	0.30	2.31	2.81×10^{-4}	6.19×10^{-4}	1	4.66×10^1	1.40×10^{-1}	1.13×10^{-5}
¹²⁰ Kr	36	84	120	0.30	2.33	3.00×10^{-4}	6.63×10^{-4}	1	4.57×10^1	1.43×10^{-1}	1.22×10^{-5}

TABLE XVIII. Same as Tables XVI and XVII, but for $B_\star = 3 \times 10^4$.

AME2020+KTUY ($B_\star = 3 \times 10^4$)											
Nuclides	Z	N	A	y_e	N/Z	$n_{\max} [\text{fm}^{-3}]$	$P_{\max} [\text{MeV}/\text{fm}^3]$	ν_{\max}	$R [\text{fm}]$	$\hbar\omega [\text{MeV}]$	$S [\text{MeV}/\text{fm}^3]$
⁶⁰ Ni	28	32	60	0.47	1.14	1.37×10^{-4}	1.56×10^{-5}	0	4.71×10^1	1.50×10^{-1}	6.54×10^{-6}
⁹⁰ Zr	40	50	90	0.44	1.25	2.88×10^{-4}	9.43×10^{-5}	0	4.21×10^1	2.08×10^{-1}	2.09×10^{-5}
⁸⁸ Sr	38	50	88	0.43	1.32	8.27×10^{-4}	1.02×10^{-3}	0	2.94×10^1	3.42×10^{-1}	7.94×10^{-5}
⁸⁶ Kr	36	50	86	0.42	1.39	1.01×10^{-3}	1.48×10^{-3}	0	2.73×10^1	3.67×10^{-1}	9.65×10^{-5}
¹²⁸ Sn	50	78	128	0.39	1.56	1.13×10^{-3}	1.54×10^{-3}	0	3.00×10^1	3.61×10^{-1}	1.26×10^{-4}
¹³⁴ Te	52	82	134	0.39	1.58	1.31×10^{-3}	2.10×10^{-3}	0	2.90×10^1	3.87×10^{-1}	1.57×10^{-4}
¹³² Sn	50	82	132	0.38	1.64	2.48×10^{-3}	7.67×10^{-3}	0	2.33×10^1	5.19×10^{-1}	3.46×10^{-4}
¹²⁸ Pd	46	82	128	0.36	1.78	2.97×10^{-3}	1.00×10^{-2}	0	2.17×10^1	5.39×10^{-1}	3.88×10^{-4}
¹²⁶ Ru	44	82	126	0.35	1.86	3.20×10^{-3}	1.11×10^{-2}	0	2.11×10^1	5.44×10^{-1}	4.01×10^{-4}
¹⁸⁸ Sm	62	126	188	0.33	2.03	3.60×10^{-3}	1.22×10^{-2}	0	2.32×10^1	5.44×10^{-1}	5.45×10^{-4}
¹⁸⁶ Nd	60	126	186	0.32	2.10	3.91×10^{-3}	1.39×10^{-2}	0	2.25×10^1	5.55×10^{-1}	5.79×10^{-4}
¹⁸⁴ Ce	58	126	184	0.32	2.17	4.60×10^{-3}	1.86×10^{-2}	0	2.12×10^1	5.88×10^{-1}	6.81×10^{-4}
¹⁸² Ba	56	126	182	0.31	2.25	4.82×10^{-3}	1.95×10^{-2}	0	2.08×10^1	5.87×10^{-1}	6.86×10^{-4}
¹⁸⁰ Xe	54	126	180	0.30	2.33	4.99×10^{-3}	1.99×10^{-2}	0	2.05×10^1	5.82×10^{-1}	6.77×10^{-4}

TABLE XIX. Same as Tables XVI–XVIII, but for $B_\star = 7 \times 10^4$.

AME2020+KTUY ($B_\star = 7 \times 10^4$)											
Nuclides	Z	N	A	y_e	N/Z	$n_{\max} [\text{fm}^{-3}]$	$P_{\max} [\text{MeV}/\text{fm}^3]$	ν_{\max}	$R [\text{fm}]$	$\hbar\omega [\text{MeV}]$	$S [\text{MeV}/\text{fm}^3]$
⁹⁰ Zr	40	50	90	0.44	1.25	1.17×10^{-3}	7.47×10^{-4}	0	2.64×10^1	4.18×10^{-1}	1.36×10^{-4}
⁸⁸ Sr	38	50	88	0.43	1.32	1.95×10^{-3}	2.28×10^{-3}	0	2.21×10^1	5.25×10^{-1}	2.49×10^{-4}
¹³⁸ Ba	56	82	138	0.41	1.46	2.47×10^{-3}	3.10×10^{-3}	0	2.37×10^1	5.55×10^{-1}	4.07×10^{-4}
¹³⁶ Xe	54	82	136	0.40	1.52	3.13×10^{-3}	5.05×10^{-3}	0	2.18×10^1	6.12×10^{-1}	5.30×10^{-4}
¹³⁴ Te	52	82	134	0.39	1.58	3.79×10^{-3}	7.30×10^{-3}	0	2.04×10^1	6.57×10^{-1}	6.45×10^{-4}
¹³² Sn	50	82	132	0.38	1.64	6.03×10^{-3}	1.88×10^{-2}	0	1.73×10^1	8.10×10^{-1}	1.13×10^{-3}
¹⁹⁶ Yb	70	126	196	0.36	1.80	6.96×10^{-3}	2.16×10^{-2}	0	1.89×10^1	8.19×10^{-1}	1.58×10^{-3}
¹⁹⁴ Er	68	126	194	0.35	1.85	7.56×10^{-3}	2.48×10^{-2}	0	1.83×10^1	8.38×10^{-1}	1.69×10^{-3}
¹⁹² Dy	66	126	192	0.34	1.91	8.10×10^{-3}	2.77×10^{-2}	0	1.78×10^1	8.51×10^{-1}	1.77×10^{-3}
¹⁹⁰ Gd	64	126	190	0.34	1.97	8.49×10^{-3}	2.94×10^{-2}	0	1.75×10^1	8.54×10^{-1}	1.80×10^{-3}
²⁴⁸ Pb	82	166	248	0.33	2.02	8.89×10^{-3}	3.03×10^{-2}	0	1.88×10^1	8.57×10^{-1}	2.20×10^{-3}
²⁵⁰ Pb	82	168	250	0.33	2.05	9.09×10^{-3}	3.12×10^{-2}	0	1.87×10^1	8.60×10^{-1}	2.24×10^{-3}
²⁵² Pb	82	170	252	0.33	2.07	9.42×10^{-3}	3.31×10^{-2}	0	1.85×10^1	8.68×10^{-1}	2.33×10^{-3}
²⁵⁴ Pb	82	172	254	0.32	2.10	1.00×10^{-2}	3.73×10^{-2}	0	1.82×10^1	8.90×10^{-1}	2.51×10^{-3}
²⁵⁶ Pb	82	174	256	0.32	2.12	1.03×10^{-2}	3.88×10^{-2}	0	1.81×10^1	8.95×10^{-1}	2.58×10^{-3}
²⁵⁸ Pb	82	176	258	0.32	2.15	1.08×10^{-2}	4.25×10^{-2}	0	1.78×10^1	9.10×10^{-1}	2.73×10^{-3}
²⁶⁰ Pb	82	178	260	0.32	2.17	1.11×10^{-2}	4.38×10^{-2}	0	1.77×10^1	9.13×10^{-1}	2.78×10^{-3}
²⁶² Pb	82	180	262	0.31	2.20	1.12×10^{-2}	4.42×10^{-2}	0	1.77×10^1	9.12×10^{-1}	2.80×10^{-3}
²⁶⁴ Pb	82	182	264	0.31	2.22	1.16×10^{-2}	4.69×10^{-2}	0	1.75×10^1	9.21×10^{-1}	2.90×10^{-3}
²⁶⁶ Pb	82	184	266	0.31	2.24	1.22×10^{-2}	5.13×10^{-2}	0	1.73×10^1	9.37×10^{-1}	3.07×10^{-3}

TABLE XX. Same as Tables XVI–XIX, but for $B_\star = 10^5$.

AME2020+KTUY ($B_\star = 10^5$)											
Nuclides	Z	N	A	y_e	N/Z	$n_{\max} [\text{fm}^{-3}]$	$P_{\max} [\text{MeV}/\text{fm}^3]$	ν_{\max}	$R [\text{fm}]$	$\hbar\omega [\text{MeV}]$	$S [\text{MeV}/\text{fm}^3]$
⁹⁰ Zr	40	50	90	0.44	1.25	2.06×10^{-3}	1.66×10^{-3}	0	2.18×10^1	5.55×10^{-1}	2.88×10^{-4}
⁸⁸ Sr	38	50	88	0.43	1.32	2.40×10^{-3}	2.23×10^{-3}	0	2.06×10^1	5.82×10^{-1}	3.28×10^{-4}
¹¹⁸ Sn	50	68	118	0.42	1.36	2.68×10^{-3}	2.57×10^{-3}	0	2.19×10^1	6.04×10^{-1}	4.45×10^{-4}
¹⁴⁰ Ce	58	82	140	0.41	1.41	3.12×10^{-3}	3.32×10^{-3}	0	2.20×10^1	6.37×10^{-1}	5.85×10^{-4}
¹³⁸ Ba	56	82	138	0.41	1.46	4.10×10^{-3}	5.98×10^{-3}	0	2.00×10^1	7.15×10^{-1}	8.01×10^{-4}
¹³⁶ Xe	54	82	136	0.40	1.52	5.05×10^{-3}	9.08×10^{-3}	0	1.86×10^1	7.76×10^{-1}	1.00×10^{-3}
¹³⁴ Te	52	82	134	0.39	1.58	5.98×10^{-3}	1.26×10^{-2}	0	1.75×10^1	8.26×10^{-1}	1.19×10^{-3}
¹³² Sn	50	82	132	0.38	1.64	7.29×10^{-3}	1.84×10^{-2}	0	1.63×10^1	8.90×10^{-1}	1.46×10^{-3}
²⁰² Os	76	126	202	0.38	1.66	8.44×10^{-3}	2.34×10^{-2}	0	1.79×10^1	9.51×10^{-1}	2.32×10^{-3}
²⁰⁰ W	74	126	200	0.37	1.70	9.21×10^{-3}	2.74×10^{-2}	0	1.73×10^1	9.77×10^{-1}	2.51×10^{-3}
¹⁹⁸ Hf	72	126	198	0.36	1.75	9.99×10^{-3}	3.15×10^{-2}	0	1.68×10^1	9.99×10^{-1}	2.68×10^{-3}
¹⁹⁶ Yb	70	126	196	0.36	1.80	1.05×10^{-2}	3.38×10^{-2}	0	1.65×10^1	1.01×10^0	2.74×10^{-3}
²⁶⁰ Th	90	170	260	0.35	1.89	1.11×10^{-2}	3.48×10^{-2}	0	1.77×10^1	1.01×10^0	3.37×10^{-3}
²⁵⁶ Ra	88	168	256	0.34	1.91	1.15×10^{-2}	3.66×10^{-2}	0	1.75×10^1	1.01×10^0	3.42×10^{-3}
²⁵⁸ Ra	88	170	258	0.34	1.93	1.17×10^{-2}	3.77×10^{-2}	0	1.74×10^1	1.02×10^0	3.48×10^{-3}
²⁷² U	92	180	272	0.34	1.96	1.24×10^{-2}	4.12×10^{-2}	0	1.74×10^1	1.03×10^0	3.81×10^{-3}
²⁷⁴ U	92	182	274	0.34	1.98	1.27×10^{-2}	4.29×10^{-2}	0	1.73×10^1	1.04×10^0	3.90×10^{-3}
²⁷⁶ U	92	184	276	0.33	2.00	1.36×10^{-2}	4.93×10^{-2}	0	1.69×10^1	1.07×10^0	4.25×10^{-3}
²⁷⁴ Th	90	184	274	0.33	2.04	1.43×10^{-2}	5.34×10^{-2}	0	1.66×10^1	1.08×10^0	4.40×10^{-3}
²⁷² Ra	88	184	272	0.32	2.09	1.51×10^{-2}	5.78×10^{-2}	0	1.63×10^1	1.09×10^0	4.54×10^{-3}
²⁷⁰ Rn	86	184	270	0.32	2.14	1.63×10^{-2}	6.64×10^{-2}	0	1.58×10^1	1.12×10^0	4.87×10^{-3}
²⁶⁸ Po	84	184	268	0.31	2.19	1.69×10^{-2}	6.91×10^{-2}	0	1.56×10^1	1.12×10^0	4.91×10^{-3}
²⁶⁴ Pb	82	182	264	0.31	2.22	1.73×10^{-2}	7.12×10^{-2}	0	1.54×10^1	1.12×10^0	4.91×10^{-3}
²⁶⁶ Pb	82	184	266	0.31	2.24	1.82×10^{-2}	7.79×10^{-2}	0	1.52×10^1	1.14×10^0	5.20×10^{-3}

TABLE XXI. Same as Tables XVI–XX, but for $B_\star = 1.4 \times 10^5$.

AME2020 + KTUY ($B_\star = 1.4 \times 10^5$)											
Nuclides	Z	N	A	y_e	N/Z	$n_{\max} [\text{fm}^{-3}]$	$P_{\max} [\text{MeV}/\text{fm}^3]$	ν_{\max}	$R [\text{fm}]$	$\hbar\omega [\text{MeV}]$	$S [\text{MeV}/\text{fm}^3]$
⁹⁰ Zr	40	50	90	0.44	1.25	2.78×10^{-3}	2.02×10^{-3}	0	1.98×10^1	6.45×10^{-1}	4.31×10^{-4}
¹¹⁶ Sn	50	66	116	0.43	1.32	3.29×10^{-3}	2.59×10^{-3}	0	2.03×10^1	6.80×10^{-1}	6.00×10^{-4}
¹⁴² Nd	60	82	142	0.42	1.37	3.89×10^{-3}	3.46×10^{-3}	0	2.06×10^1	7.25×10^{-1}	8.24×10^{-4}
¹⁴⁰ Ce	58	82	140	0.41	1.41	5.30×10^{-3}	6.94×10^{-3}	0	1.85×10^1	8.30×10^{-1}	1.19×10^{-3}
¹³⁸ Ba	56	82	138	0.41	1.46	6.39×10^{-3}	1.02×10^{-2}	0	1.73×10^1	8.93×10^{-1}	1.44×10^{-3}
²⁰⁸ Pb	82	126	208	0.39	1.54	9.58×10^{-3}	2.18×10^{-2}	0	1.73×10^1	1.06×10^0	3.08×10^{-3}
²⁰⁶ Hg	80	126	206	0.39	1.57	1.06×10^{-2}	2.63×10^{-2}	0	1.67×10^1	1.10×10^0	3.38×10^{-3}
²⁰⁴ Pt	78	126	204	0.38	1.62	1.17×10^{-2}	3.18×10^{-2}	0	1.61×10^1	1.14×10^0	3.71×10^{-3}
²⁰² Os	76	126	202	0.38	1.66	1.29×10^{-2}	3.84×10^{-2}	0	1.55×10^1	1.17×10^0	4.08×10^{-3}
²⁸⁸ Rf	104	184	288	0.36	1.77	1.41×10^{-2}	4.04×10^{-2}	0	1.69×10^1	1.18×10^0	5.38×10^{-3}
²⁸⁴ No	102	182	284	0.36	1.78	1.44×10^{-2}	4.16×10^{-2}	0	1.68×10^1	1.18×10^0	5.39×10^{-3}
²⁸⁶ No	102	184	286	0.36	1.80	1.50×10^{-2}	4.51×10^{-2}	0	1.66×10^1	1.20×10^0	5.66×10^{-3}
²⁸² Fm	100	182	282	0.35	1.82	1.52×10^{-2}	4.60×10^{-2}	0	1.64×10^1	1.20×10^0	5.64×10^{-3}
²⁸⁴ Fm	100	184	284	0.35	1.84	1.54×10^{-2}	4.69×10^{-2}	0	1.64×10^1	1.20×10^0	5.71×10^{-3}
³⁰⁸ Hs	108	200	308	0.35	1.85	1.64×10^{-2}	5.23×10^{-2}	0	1.65×10^1	1.23×10^0	6.48×10^{-3}
³⁰⁶ Sg	106	200	306	0.35	1.89	1.75×10^{-2}	5.90×10^{-2}	0	1.61×10^1	1.26×10^0	6.86×10^{-3}
³⁰⁴ Rf	104	200	304	0.34	1.92	1.86×10^{-2}	6.58×10^{-2}	0	1.57×10^1	1.28×10^0	7.23×10^{-3}
³⁰² No	102	200	302	0.34	1.96	1.96×10^{-2}	7.20×10^{-2}	0	1.54×10^1	1.30×10^0	7.52×10^{-3}
³⁰⁰ Fm	100	200	300	0.33	2.00	2.08×10^{-2}	8.03×10^{-2}	0	1.51×10^1	1.32×10^0	7.92×10^{-3}
²⁹⁸ Cf	98	200	298	0.33	2.04	2.20×10^{-2}	8.78×10^{-2}	0	1.48×10^1	1.34×10^0	8.24×10^{-3}
²⁹⁶ Cm	96	200	296	0.32	2.08	2.32×10^{-2}	9.60×10^{-2}	0	1.45×10^1	1.36×10^0	8.58×10^{-3}
²⁹⁴ Pu	94	200	294	0.32	2.13	2.43×10^{-2}	1.03×10^{-1}	0	1.42×10^1	1.37×10^0	8.81×10^{-3}
²⁹² U	92	200	292	0.32	2.17	2.54×10^{-2}	1.10×10^{-1}	0	1.40×10^1	1.38×10^0	9.05×10^{-3}
²⁹⁰ Th	90	200	290	0.31	2.22	2.64×10^{-2}	1.16×10^{-1}	0	1.38×10^1	1.39×10^0	9.19×10^{-3}